


CRL4^{AMBRA1} targets Elongin C for ubiquitination and degradation to modulate CRL5 signaling

Si-Han Chen^{1,2,3,4}, Gwendolyn M Jang^{1,3,4}, Ruth Hüttenhain^{1,3,4}, David E Gordon^{1,3,4}, Dan Du⁵ , Billy W Newton^{1,3,4}, Jeffrey R Johnson^{1,3,4}, Joseph Hiatt^{6,7,8,9}, Judd F Hultquist^{1,3,4}, Tasha L Johnson^{1,3,4}, Yi-Liang Liu¹⁰, Lily A Burton¹¹, Jordan Ye^{12,13}, Kurt M Reichermeier¹⁴, Robert M Stroud^{3,10}, Alexander Marson^{3,8,9,15,16,17}, Jayanta Debnath^{12,13}, John D Gross^{3,11}  & Nevan J Krogan^{1,3,4,13,*} 

Abstract

Multi-subunit cullin-RING ligases (CRLs) are the largest family of ubiquitin E3 ligases in humans. CRL activity is tightly regulated to prevent unintended substrate degradation or autocatalytic degradation of CRL subunits. Using a proteomics strategy, we discovered that CRL4^{AMBRA1} (CRL substrate receptor denoted in superscript) targets Elongin C (ELOC), the essential adapter protein of CRL5 complexes, for polyubiquitination and degradation. We showed that the ubiquitin ligase function of CRL4^{AMBRA1} is required to disrupt the assembly and attenuate the ligase activity of human CRL5^{SOC3} and HIV-1 CRL5^{VIF} complexes as AMBRA1 depletion leads to hyperactivation of both CRL5 complexes. Moreover, CRL4^{AMBRA1} modulates interleukin-6/STAT3 signaling and HIV-1 infectivity that are regulated by CRL5^{SOC3} and CRL5^{VIF}, respectively. Thus, by discovering a substrate of CRL4^{AMBRA1}, ELOC, the shared adapter of CRL5 ubiquitin ligases, we uncovered a novel CRL cross-regulation pathway.

Keywords AMBRA1; cullin-RING ligase; HIV infection; interleukin-6; ubiquitin

Subject Categories Autophagy & Cell Death; Post-translational Modifications, Proteolysis & Proteomics; Systems & Computational Biology

DOI 10.15252/emboj.201797508 | Received 5 June 2017 | Revised 26 July 2018 |

Accepted 1 August 2018 | Published online 30 August 2018

The EMBO Journal (2018) 37: e97508

Introduction

Ubiquitination is a post-translational modification that regulates many cellular processes, such as protein degradation, intracellular trafficking, and protein localization (Hicke & Dunn, 2003). It involves transferring ubiquitin molecules from an activating enzyme E1 to a conjugating enzyme E2 and then to a ligase enzyme E3. The latter contains a substrate-recognizing moiety, or substrate receptor (SR), that recognizes and targets specific protein substrates for either mono- or polyubiquitination. Polyubiquitination primarily directs substrates to the ubiquitin proteasome pathway for degradation, affecting cell cycle progression, innate immunity, and viral pathogenesis (Frescas & Pagano, 2008; Mahon *et al*, 2014).

Cullin-RING ligases (CRLs) are the largest family of ubiquitin E3 ligases, and humans have more than seven CRL subfamilies. Their molecular architecture includes a cullin scaffold (CUL), a RING-box protein (RBX1 or RBX2) for recruiting an E2, one or more adapter proteins, and an interchangeable SR (Petroski & Deshaies, 2005). CRLs form multi-subunit complexes that distinctly fine-tune E3 ligase activity. These complexes are activated by covalent attachment of the ubiquitin-like protein NEDD8 to the cullins in a process called NEDDylation (Duda *et al*, 2008). Hyperactivation of CRL complexes is linked to autocatalytic degradation of SRs, particularly in the absence of their substrates, which leads to disassembly and deactivation of CRL complexes (Zhou & Howley, 1998). This activity can be controlled by master regulators, such as the de-neddylator

1 Department of Cellular and Molecular Pharmacology, California Institute for Quantitative Biosciences, University of California, San Francisco, San Francisco, CA, USA

2 Biophysics Graduate Program, University of California, San Francisco, San Francisco, CA, USA

3 Quantitative Biosciences Institute (QBI), University of California, San Francisco, San Francisco, CA, USA

4 Gladstone Institutes, San Francisco, CA, USA

5 Department of Cell and Tissue Biology, University of California, San Francisco, San Francisco, CA, USA

6 Medical Scientist Training Program, University of California, San Francisco, San Francisco, CA, USA

7 Biomedical Sciences Graduate Program, University of California, San Francisco, San Francisco, CA, USA

8 Department of Microbiology and Immunology, University of California, San Francisco, San Francisco, CA, USA

9 Diabetes Center, University of California, San Francisco, San Francisco, CA, USA

10 Department of Biochemistry and Biophysics, University of California, San Francisco, San Francisco, CA, USA

11 Department of Pharmaceutical Chemistry, University of California, San Francisco, San Francisco, CA, USA

12 Department of Pathology, University of California, San Francisco, San Francisco, CA, USA

13 Helen Diller Family Comprehensive Cancer Center, University of California, San Francisco, San Francisco, CA, USA

14 California Institute of Technology, Pasadena, CA, USA

15 Division of Infectious Diseases and Rheumatology, University of California, Berkeley, Berkeley, CA, USA

16 Innovative Genomics Institute, University of California, Berkeley, Berkeley, CA, USA

17 Chan Zuckerberg Biohub, San Francisco, CA, USA

*Corresponding author. Tel: +1 415 476 2980; E-mail: nevan.krogan@ucsf.edu

COP9 signalosome (CSN), the cullin-associated protein CAND1, and the RBX1-binding protein glomulin, to prevent premature disassembly of CRL complexes and unintended degradation of their substrates (Wee *et al*, 2005; Schmidt *et al*, 2009; Tron *et al*, 2012).

Interestingly, some CRL complexes regulate the activity of other CRLs by targeting their subunits for polyubiquitination and degradation. For example, CRL1^{FBXO11} targets the CRL4 SR CDT2 for degradation to control cell cycle progression (Abbas *et al*, 2013; Rossi *et al*, 2013). However, there are limited data detailing how crosstalk between CRLs affects the complex and heterologous regulation of CRL activity.

CRL4 ubiquitin E3 ligases regulate DNA-damage repair and cell cycle progression. Many CRL4 SRs target DNA lesions and cell cycle regulators for ubiquitination and degradation (Fischer *et al*, 2011), while others regulate cellular processes in the cytoplasm (Petzold *et al*, 2016). The CRL4 SR AMBRA1 (CRL4^{AMBRA1}) is primarily a cytoplasmic protein that regulates autophagy by modulating the Beclin1-Vps34 complex (Maria Fimia *et al*, 2007; Xia *et al*, 2013) or CRL5-mediated DEPTOR degradation (Antonoli *et al*, 2014). Besides Beclin1, AMBRA1's function as a SR of CRL4 and its full range of substrates remain largely unexplored. Interestingly, AMBRA1 also interacts with HIV-1 VIF (Jäger *et al*, 2011a), a viral SR that hijacks CRL5 to degrade antiviral APOBEC3 proteins (Yu *et al*, 2003), suggesting that AMBRA1 may influence CRL crosstalk.

Based on the potential role of AMBRA1 in CRL crosstalk and our lack of understanding of CRL4^{AMBRA1} functions, we sought to identify the substrates of CRL4^{AMBRA1} using quantitative proteomic approaches and to confirm changes in their polyubiquitination and protein level in an AMBRA1-dependent manner.

Results

Crosstalk between CRL5^{VIF} and CRL4^{AMBRA1} complexes

Using affinity tag purification–mass spectrometry (AP-MS), we previously constructed a comprehensive and unbiased HIV-1–human protein–protein interaction map using a quantitative scoring method that accounts for abundance, reproducibility, and specificity of co-purified human proteins (Jäger *et al*, 2011a). In this study, we identified seven high-confidence interactions between the viral VIF protein and human proteins in both HEK293 and Jurkat T cells (Fig 1A). Six of these interactions represent viral hijacking of the

human ubiquitin E3 ligase CRL5 by VIF to attain successful viral replication (Yu *et al*, 2003), including the core components of CRL5—CUL5, RBX2, Elongin B (ELOB), and Elongin C (ELOC). CUL2 is another VIF-interacting cullin scaffold protein that also binds to the adapter proteins ELOB and ELOC, although its connection with VIF is unclear. CBF β , a VIF co-factor, is critical for CRL5^{VIF} complex formation (Jäger *et al*, 2011c; Guo *et al*, 2014). AMBRA1 was among the seven human proteins that co-purified with VIF, but its connection to VIF and HIV-1 biology remained obscure. We confirmed VIF-AMBRA1 interaction via reciprocal immunoprecipitations (IPs) using both antibodies against AMBRA1 (Fig EV1) as well as overexpressed tagged AMBRA1 (Appendix Fig S1). VIF also interacts with DNA damage-binding protein 1 (DDB1) and AMBRA1 during HIV-1 infection (Luo *et al*, 2016), but the function of these interactions remains unknown. Previous work revealed that AMBRA1 is involved in autophagy; however, we found that overexpression of VIF did not affect levels of LC3, a readout of autophagy function (Klionsky *et al*, 2016; Fig EV2).

To further understand AMBRA1's function, we sought to determine its interaction partners using AP-MS in HEK293T cells. We confirmed that AMBRA1 interacts with components of the CRL4 complex, as previously described (Jin *et al*, 2006), as well as two adapter proteins required for CRL5 and CRL2 (CRL5/2) complexes, ELOB and ELOC (Fig 1B; Table EV1). We also performed double IPs using VIF and AMBRA1 to verify their interaction and identify co-purified proteins (Jäger *et al*, 2011b). In this experiment, VIF and AMBRA1 were affinity-tagged with 2X-Strep and 3X-Flag, respectively, co-expressed in HEK293T cells, sequentially purified, and analyzed by mass spectrometry (Fig 1C). We found that adapter proteins of both CRL5^{VIF} and CRL4^{AMBRA1}—including ELOB, ELOC, and DDB1—were enriched in the double IPs, as well as the VIF co-factor CBF β (Jäger *et al*, 2011c). However, neither the scaffold proteins nor the RING-box proteins co-purified with VIF and AMBRA1 (Fig 1D; Table EV2). These data strongly suggested that physical crosstalk exists between CRL5^{VIF} and CRL4^{AMBRA1} complexes.

AMBRA1 suppresses CRL5^{VIF}-mediated APOBEC3G degradation and modulates HIV-1 infectivity

Based on the association between AMBRA1 and components of CRL5^{VIF}, we investigated whether AMBRA1 affects CRL5^{VIF} function and HIV-1 infectivity. CRL5^{VIF} targets APOBEC3G (A3G) for degradation during HIV-1 infection (Yu *et al*, 2003), and A3G belongs to

Figure 1. The interconnection between CRL4^{AMBRA1} and CRL5^{VIF} complexes.

- A Network representation of human VIF protein–protein interactions, recreated from our published data (Jäger *et al*, 2011a). VIF AP-MS was performed in HEK293 cells and Jurkat T cells, and scored by Mass spectrometry interaction STatistics (MiST), a scoring system optimally designed for host–pathogen protein–protein interaction datasets. The orange color range and size of green ringed nodes represent MiST scores of identified VIF–human interactions in HEK293 and Jurkat cells, respectively. The red ringed node denotes the affinity-tagged bait protein (VIF). Interactors with HEK293 or Jurkat that had MiST scores below 0.75 were colored in gray or rendered in rectangles, respectively. Dash–line–circled interactors represent the CRL5^{VIF} complex, with CUL2 being another cullin scaffold that may replace CUL5. AMBRA1 was identified as a strong interactor in both HEK293 and Jurkat cells (arrow).
- B Network representation of AMBRA1-interacting proteins from 12 independent AP-MS experiments performed in HEK293T cells transfected with FLAG-tagged AMBRA1. AP-MS scoring was performed with Comparative Proteomic Analysis Software Suite (CompPASS; Sowa *et al*, 2009). The orange color range represents CompPASS scores of individual interactions. Dashed lines enclose components of CRL5/2 and CRL4 complexes, respectively. See also Table EV1.
- C Schematic of VIF-AMBRA1 tandem IP. Strep-tagged VIF and FLAG-tagged AMBRA1 were co-expressed in HEK293T cells. Cell lysates were subjected to Strep, followed by FLAG-affinity purifications.
- D Proteins identified in VIF-AMBRA1 tandem IPs in three independent experiments. Protein abundance was represented by the percentage of identified peptides over the length of the protein sequence (protein coverage %). Of note, DDA1 was only identified in one of the three experiments. Bar graph represented mean \pm SEM, $n = 3$. See also Table EV2.

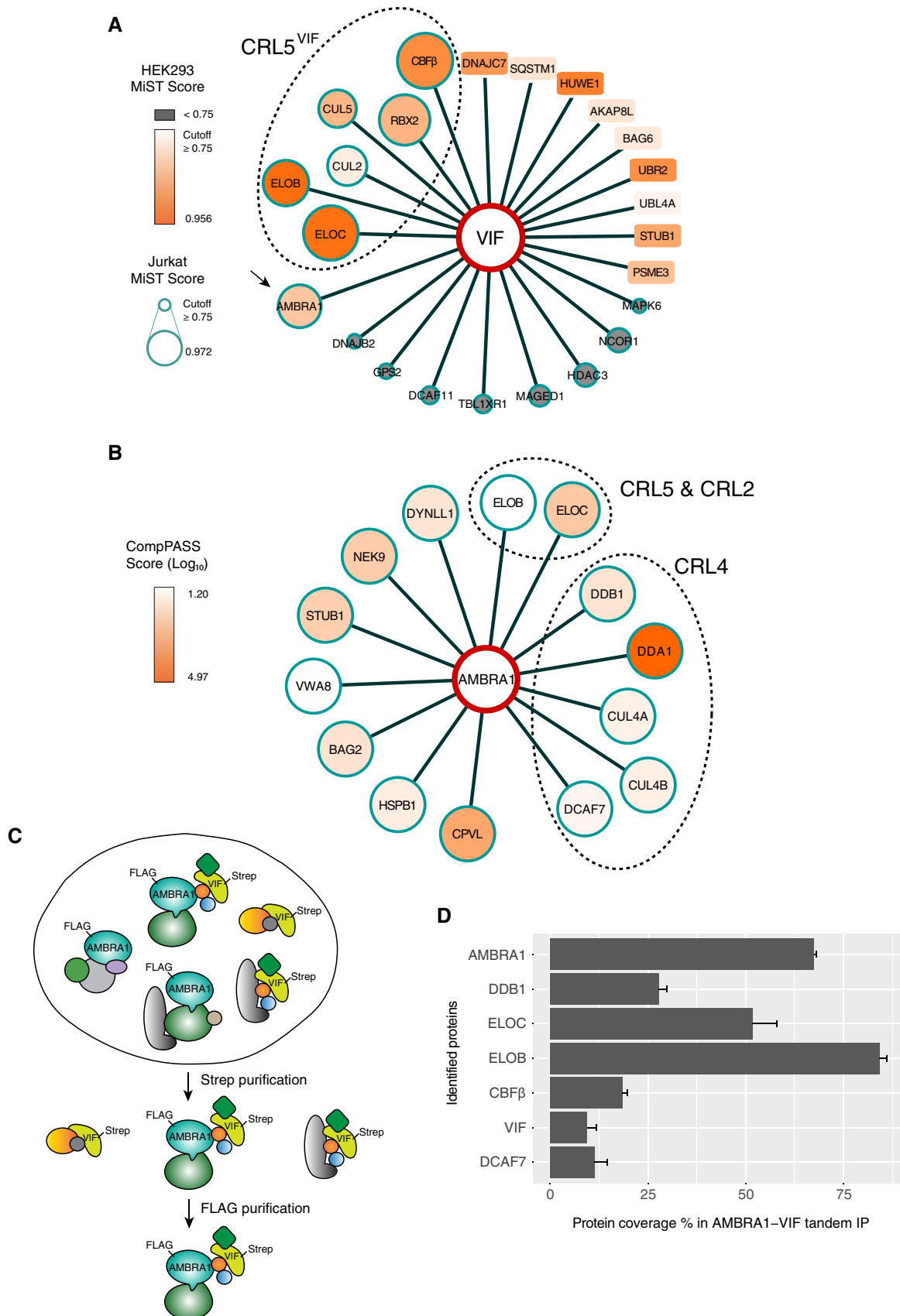


Figure 1.

the APOBEC3 family of cytidine deaminases, virus-induced restriction factors that can be encapsidated to virions and cause hypermutation in viral genomes (Lecossier *et al*, 2003). When HIV-1 VIF fails to neutralize A3G, unsuccessful infection occurs. To reduce AMBRA1 protein level and study its influence on HIV-1 infectivity, we disrupted the *AMBRA1* gene in human primary T cells with Cas9 ribonucleoproteins (RNPs) and then infected them with HIV-1 NL4-3 carrying an IRES-GFP reporter (*Nef:GFP*; Hultquist *et al*, 2016). We found that AMBRA1-depleted cells were more permissive to HIV-1 infection in a manner dependent on the efficiency of protein depletion (Fig 2A and Appendix Fig S2), a phenotype consistent with enhanced CRL5^{VIF} activity. In the same experiment, we included CXCR4 depletion as a control that blocks HIV-1 entry and reduces viral infectivity (Fig 2A and Appendix Fig S2; Hultquist *et al*, 2016). Furthermore, to understand whether AMBRA1 modulates HIV-1 infectivity through the CRL5 pathway, we co-depleted AMBRA1 with either ELOB or ELOC in primary T cells and then carried out the infection experiments (Fig 2B). Both cases showed reduced viral infectivity, the extent of which is similar to ELOB or ELOC single knockdown (Fig 2B). This genetic suppression implies that the increased viral infectivity by AMBRA1 knockdown relies on the presence of ELOB and ELOC.

Although these infection data indicate that AMBRA1 may be a restriction factor, we did not find any significant changes in infectivity in AMBRA1-overexpressing cells (Fig EV3A). In this experiment, we infected SupT11-APOBEC3G cells that overexpress mCherry, AMBRA1, or an AMBRA1 mutant (Δ H AMBRA1) that lacks a key region for CRL4^{AMBRA1} complex formation, with Vsvg-pseudotyped HIV-1 reporter viruses, *Nef:GFP* or *Gag-GFP*. Interestingly, we found that AMBRA1 is downregulated in both endogenous and overexpressed settings during HIV-1 infection, and Δ H AMBRA1 mutant is insensitive to virally induced downregulation (Fig EV3B and C). Our findings suggest that AMBRA1 negatively impacts HIV-1 infection and is antagonized by the virus through a yet-unclear mechanism.

We also showed that AMBRA1 depletion in HEK293T cells via the CRISPR/Cas9 system enhanced VIF-mediated A3G degradation in co-transfection experiments (Appendix Fig S4A and B). This increased clearance was reversed by re-expression of AMBRA1 and unaffected in the absence of VIF, regardless of AMBRA1 levels (Appendix Fig S4C). These collective results indicated that AMBRA1 modulates CRL5^{VIF} activity to regulate A3G degradation and affects HIV-1 infectivity. AMBRA1 interacts with ELOB and ELOC (abbreviated ELOBC in this study), which we hypothesized might influence CRL5^{VIF} function. Interestingly, overexpression of ELOBC phenocopied AMBRA1 reduction, supporting that ELOBC can regulate CRL5^{VIF} function, and thereby A3G levels (Appendix Fig S4D). These data imply that AMBRA1 regulates CRL5^{VIF} activity that correlates with perturbations in A3G degradation.

Comparative proteomics reveals ELOC is a substrate for CRL4^{AMBRA1}

Because components of CRL5^{VIF} and CRL4^{AMBRA1} interact with each other, we hypothesized that AMBRA1 may regulate CRL5^{VIF} activity through the CRL4^{AMBRA1} complex. To comprehensively address our hypothesis, we sought to identify the substrates of CRL4^{AMBRA1}. In a CRL4 complex, DDB1 mediates the interaction between CUL4A/B and SR of CRL4, also known as DDB1- and CUL4-associated factor (DCAF; He *et al*, 2006). DCAF-bound proteolytic substrates can be

stabilized by abolishing their association with the CRL4 catalytic core (Fig 3A; Decorsière *et al*, 2016). DCAFs share a semi-conserved helical region that directly binds to the DDB1 double β -propeller pocket (Angers *et al*, 2006; Fischer *et al*, 2011; Appendix Fig S5A). We reduced AMBRA1's DDB1-binding region to an N-terminal helix motif that aligns with the DDB1-binding region of other DCAFs. Using IP and immunoblotting, we showed that deleting either a partial (1–22 amino acids; AMBRA1 Δ H22) or complete (1–43 amino acids; AMBRA1 Δ H43) region of the predicted DDB1-binding sequence abolished AMBRA1 binding to DDB1 and CUL4A, a pattern that we also observed in the presence of VIF (Fig 3B).

Next, we hypothesized that VIF may sensitize CRL4^{AMBRA1} to degradation of certain substrates. Using AP-MS, we quantitatively compared the interactors of wild-type (WT) and mutant (Δ H22 and Δ H43) AMBRA1 in the presence of VIF. Reduction in the DDB1-binding region of AMBRA1 resulted in both the loss and gain of protein interactions (Fig 3C and Appendix Fig S5B; Table EV3). Specifically, Δ H22 and Δ H43 AMBRA1 reduced several interactions, including CUL4A/B and RBX1, which form the catalytic core of CRL4, the CRL4 adapter proteins DDB1 and DDA1 (Olma *et al*, 2009), as well as subunits of the COP9 signalosome (e.g., CSN1, CSN2, and CSN4) that are involved in de-NEDDylation of cullins (Enchev *et al*, 2012; Lingaraju *et al*, 2014).

Furthermore, the mutant AMBRA1 proteins formed more stable interactions with several proteins, including ELOC, which showed more than 1.5-fold stronger binding to both Δ H mutants compared to the WT. Similar results were observed using AP-MS in the absence of VIF (Appendix Fig S5C in the presence of VIF and Appendix Fig S5D in the absence of VIF). We confirmed the differential ELOC binding by quantifying immunoblots (Fig 3D), which showed enhanced co-purification with Δ H mutants. In contrast to AMBRA1, the CRL4 SR DCAF1 did not associate with ELOC, supporting that ELOC specifically binds to AMBRA1 (Fig 3B).

Notably, while the Δ H22 AMBRA1 could not bind to DDB1 and CUL4A/B, another helical region with a degenerate protein sequence may affect their interactions, such as with other DCAFs (Fischer *et al*, 2011, 2014). Thus, we used Δ H43 or Δ H34 (abbreviated Δ H) for subsequent functional experiments. Δ H34 contains a larger deletion than Δ H22 AMBRA1, and it loses interactions with DDB1 and CUL4A/B (Appendix Fig S5A).

Biochemical validation that CRL4^{AMBRA1} regulates ELOC

Using co-IP studies, we found that AMBRA1 specifically interacts with CUL4A/B and not CUL5, suggesting that AMBRA1 is not an integral part of CRL5 (Fig 4A), but it may regulate CRL5 (Antonoli *et al*, 2014). We also found that ELOC does not interact with either of the CRL4 scaffold proteins (CUL4A and CUL4B), indicating that it is not a component of CRL4 (Fig 4A). We also confirmed that IP of endogenous AMBRA1 co-purified endogenous ELOC (Fig 4B) and discovered that both AMBRA1 and ELOC are largely cytoplasmic (Fig EV4A). ELOC shares 30% sequence identity with the CRL1 adapter SKP1, which does not interact with AMBRA1, supporting that AMBRA1 specifically binds ELOC (Appendix Fig S6A and B). We further showed that AMBRA1 amino acids 735–1,208 are critical for ELOC binding (Appendix Fig S7A and B), whereas deletion of ELOC C-terminal sequence 91–112 blocks both AMBRA1 and CUL5 interactions (Appendix Fig S7C).

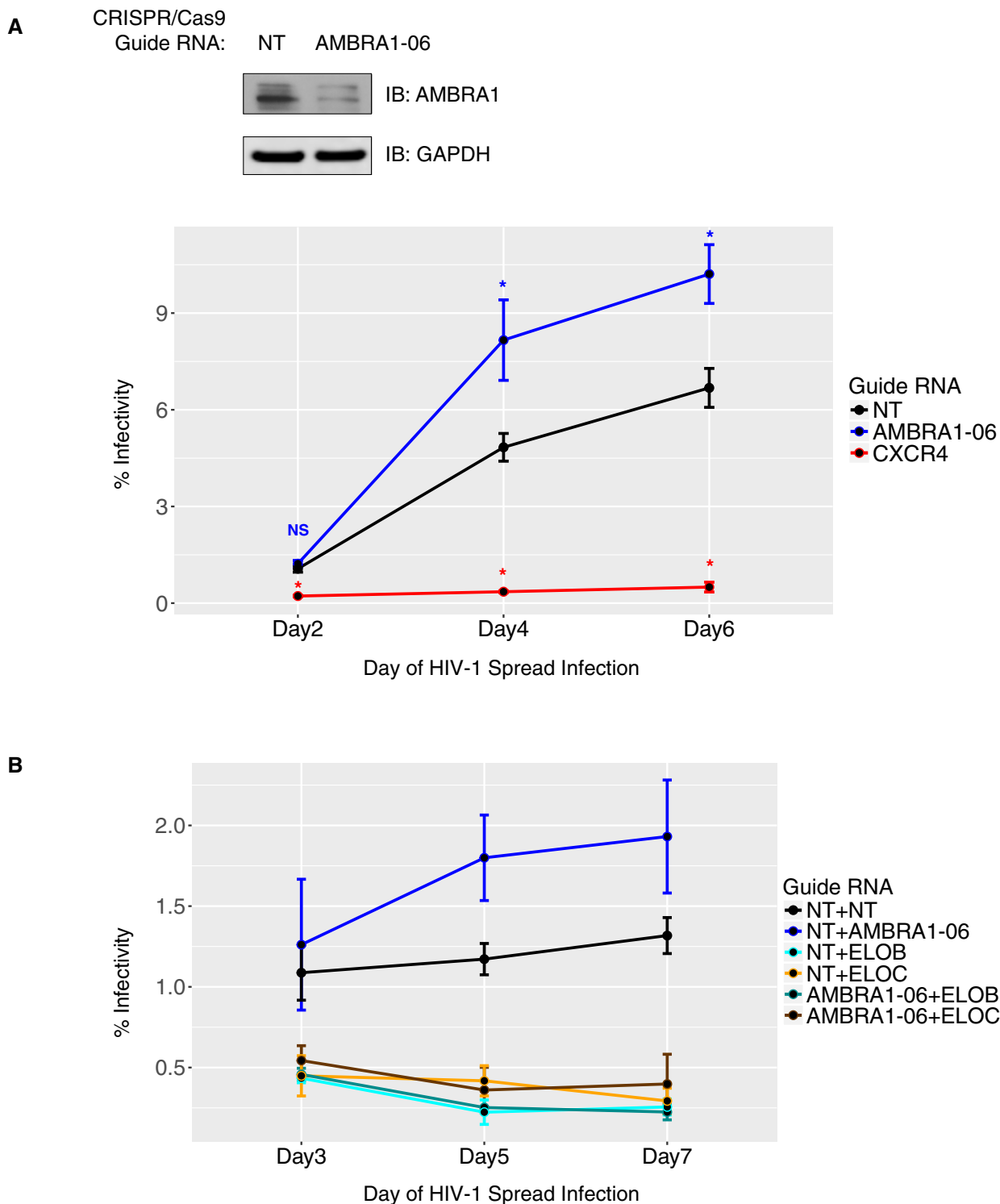


Figure 2. AMBRA1 modulates HIV-1 infectivity.

A, B HIV-1 infection in human primary CD4⁺ T cells with the indicated single (A) or double (B) gene knockout. Activated human primary CD4⁺ T cells were electroporated with pre-mixed Cas9 ribonucleoproteins (RNPs) to mediate knockout and followed by infection with HIV-1 NL4-3 that carries an IRES-GFP reporter downstream of *nef*. Cells were infected with an MOI that resulted in 1% of GFP expression in the non-targeting (NT) cells at the first timepoints, and the spread of HIV-1 was further monitored on different days. Percent infectivity was measured by percent GFP-positive population over the healthy T-cell population using flow cytometry. Statistical analysis of paired comparisons between NT and the gene of interest was carried out by Mann–Whitney–Wilcoxon test (* $P < 0.05$; NS: not significant). Each data point represents mean \pm SEM, $n = 3$. Protein depletion was verified by immunoblot.

Source data are available online for this figure.

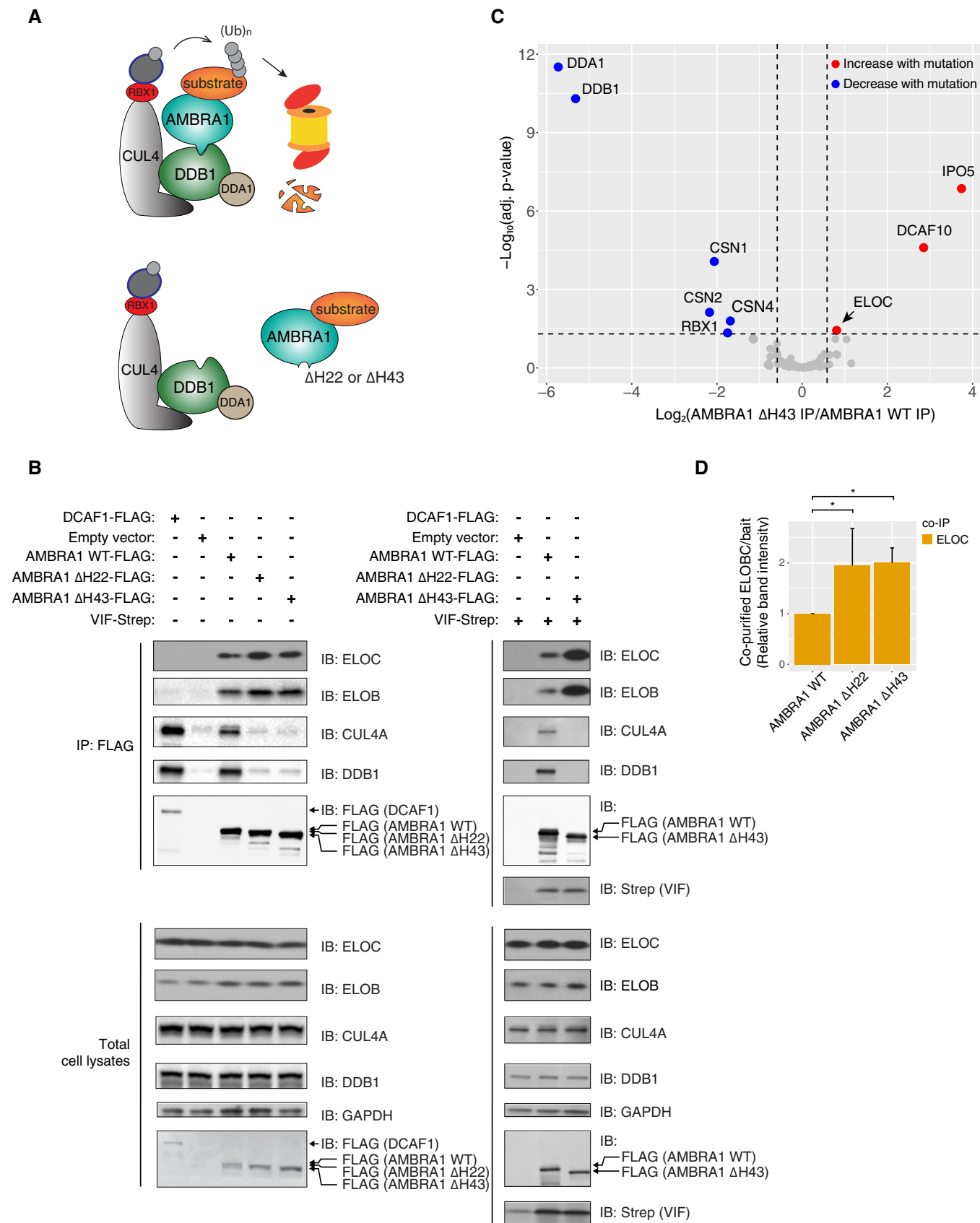


Figure 3.

Figure 3. Comparative proteomics identify proteolytic substrates of CRL4^{AMBRA1}.

- A Strategy to identify CRL4^{AMBRA1} substrates. Depicted in cartoon, deletion of the predicted helical region may inhibit binding of AMBRA1 to DDB1 and the rest of the complex, stabilizing the substrate(s).
- B Immunoblots showing loss of CUL4 and DDB1 interactions by removing the predicted helical region of AMBRA1 and confirming enhanced binding of identified substrates (see Fig 3C) by the mutants. Empty vector, FLAG-tagged DCAF1, AMBRA1 WT, ΔH22, and ΔH43 were affinity-purified with anti-FLAG beads from transfected HEK293T cells with or without VIF-Strep co-transfection. IP and input lysates were analyzed by immunoblot.
- C Volcano plot showing gain (red) and loss (blue) of interactions by ΔH43 mutant compared to WT AMBRA1 in three independent AP-MS experiments. The proteomic screen was performed on HEK293T cells co-expressing VIF-Strep and FLAG-tagged bait proteins. X-axis denotes log₂-fold change (FC) of ΔH43-bound proteins to WT-bound proteins; vertical dash lines delineate FC > 1.5. Y-axis denotes -log₁₀-adjusted P-value to indicate statistical significance of each interactor; horizontal dashed line delineates < 0.05 adjusted P-values (Choi *et al*, 2014). Note that CUL4A and CUL4B were not detected in ΔH43 proteomic data, resulting in infinity values and thus not shown on the plot. See also Table EV3.
- D Densitometric quantification of co-purified ELOC-band intensity relative to the purified FLAG-bait intensity on immunoblot. AMBRA1 WT, ΔH22, and ΔH43 FLAG IPs were performed on HEK293T cells co-expressing the FLAG-tagged bait proteins with VIF-Strep. Statistical analysis of paired comparisons was carried out by Mann–Whitney–Wilcoxon test (*P < 0.05). Bar graph represents mean ± SEM, n = 3.

Source data are available online for this figure.

To test whether CRL4^{AMBRA1} targets ELOC for polyubiquitination and degradation, we assessed whether ELOC is a proteasomal substrate affected by AMBRA1 levels. We generated a clonal HEK293T cell line that stably expresses FLAG-tagged ELOC and performed denaturing IP either on total ubiquitin or FLAG (Fig 4C and D). We found that proteasome inhibition with MG132 increased the levels of ELOC protein and its polyubiquitination. When pulling down total ubiquitin, more ELOC was co-purified from cells treated with MG132 (Fig 4C). In addition, ELOC has more ubiquitin incorporation in MG132-treated cells (Fig 4D). Similar results were observed when myc-tagged ubiquitin was exogenously expressed (Appendix Fig S8A). Replacing the WT ubiquitin with the K48R mutant largely diminished ELOC polyubiquitination (Appendix Fig S8B), indicating that the ELOC is modified at least partly with K48-linked chains, a common ubiquitin linkage type for proteasome-mediated protein turnover. Importantly, when expression of AMBRA1 was knocked down with siRNA, ELOC polyubiquitination was decreased (Fig 4E and Appendix Fig S9). Interestingly, a previous study using ubiquitin-remnant profiling identified an ELOC K32-containing peptide which accumulated after prolonged proteasomal inhibition (Kim *et al*, 2011). Here, we found that the ELOC K32R mutation phenocopies AMBRA1 knockdown, abolishing ELOC polyubiquitination, suggesting that CRL4^{AMBRA1} mediates ELOC polyubiquitination on the K32 residue (Fig 4F).

The level of ELOC protein also increased when AMBRA1 was knocked down, which paralleled the degree of AMBRA1 depletion by shRNAs (Fig 5A), a result consistent with a cycloheximide (CHX) pulse-chase experiment, where protein translation was blocked by CHX, with and without AMBRA1 following cytoplasmic

enrichment (Fig EV4A and B). As a control, we demonstrated that knockdown of AMBRA1 stabilizes p62/SQSTM, an autophagic cargo that is stabilized when autophagy is inhibited (Maria Fimia *et al*, 2007; Klionsky *et al*, 2016). Additionally, despite ELOB accumulating with AMBRA1 depletion, it did not produce MG132-dependent polyubiquitination (Appendix Fig S8A). Thus, because ELOC and ELOB form a strong hydrophobic heterodimer, AMBRA1 may indirectly affect ELOB by interacting with and regulating ELOC (Stebbins *et al*, 1999). Also, we confirmed that the accumulation of ELOB in AMBRA1-knockdown cells was not a result of mRNA expression (Appendix Fig S10). Furthermore, treating AMBRA1-depleted HEK293T cells with MG132 or the inhibitor of NEDD8-activating enzyme MLN4924 did not further accumulate ELOC, indicating that AMBRA1 regulates ELOC level through proteasomal and CRL-dependent pathways (Fig 5B). To test the implication of CRL4 in regulating ELOC, we examined ELOC protein levels following DDB1 knockdown and found significant stabilization of ELOC (Fig 5C). Furthermore, we saw a similar result when using a knockout cell line of CUL4A (Appendix Fig S11A and B), where ELOC was further stabilized when CUL4B was knocked down with siRNA (Fig 5D). These data collectively demonstrate that ELOC is polyubiquitinated and degraded in a CRL4^{AMBRA1}-dependent manner.

To test whether ELOC accumulation occurs independently of autophagy, we examined ELOC levels after knocking down expression of either ATG7 or ATG12, two genes critically involved in autophagy (Geng & Klionsky, 2008; Appendix Fig S11C and D). Neither of these perturbations resulted in ELOC accumulation, supporting the idea that AMBRA1 regulates ELOC independently of the autophagy pathway (Fig EV4C and D).

Figure 4. ELOC is a ubiquitination substrate targeted by CRL4^{AMBRA1}.

- A Cullin specificity for AMBRA1 and ELOC. FLAG-tagged cullins were expressed in HEK293T cells and affinity-purified to examine co-purified AMBRA1, ELOC, and ELOB by immunoblot.
- B Endogenous ELOC co-purified with endogenous AMBRA1. HEK293T cell lysates were collected and incubated with 10 μg of either rabbit IgG or AMBRA1 antibody (Millipore). IP and input lysates were examined by immunoblot.
- C, D Increased ELOC polyubiquitination by proteasome inhibition. HEK293T cells stably expressing FLAG-ELOC were treated with DMSO or 5 μM MG132 for 6 h. Cell lysates were incubated with anti-ubiquitin TUBE1 agarose (C) or anti-FLAG beads (D). IP and total cell lysates were examined by immunoblot.
- E Elimination of ELOC polyubiquitination in AMBRA1-depleted cells. HEK293T cells expressing FLAG-ELOC or FLAG-SKP1 were pre-treated with 10 nM of non-targeting (siNT) or AMBRA1 (siAMBRA1) siRNA and transfected with myc-ubiquitin, followed by MG132 treatment and denaturing IP using anti-FLAG beads. IP and input lysates were examined by immunoblot.
- F ELOC K32R mutation decreases ELOC polyubiquitination. HEK293T cells stably expressing WT or K32R FLAG-ELOC were transfected with myc-ubiquitin and followed by denaturing IP. IP and input lysates were examined by immunoblot.

Source data are available online for this figure.

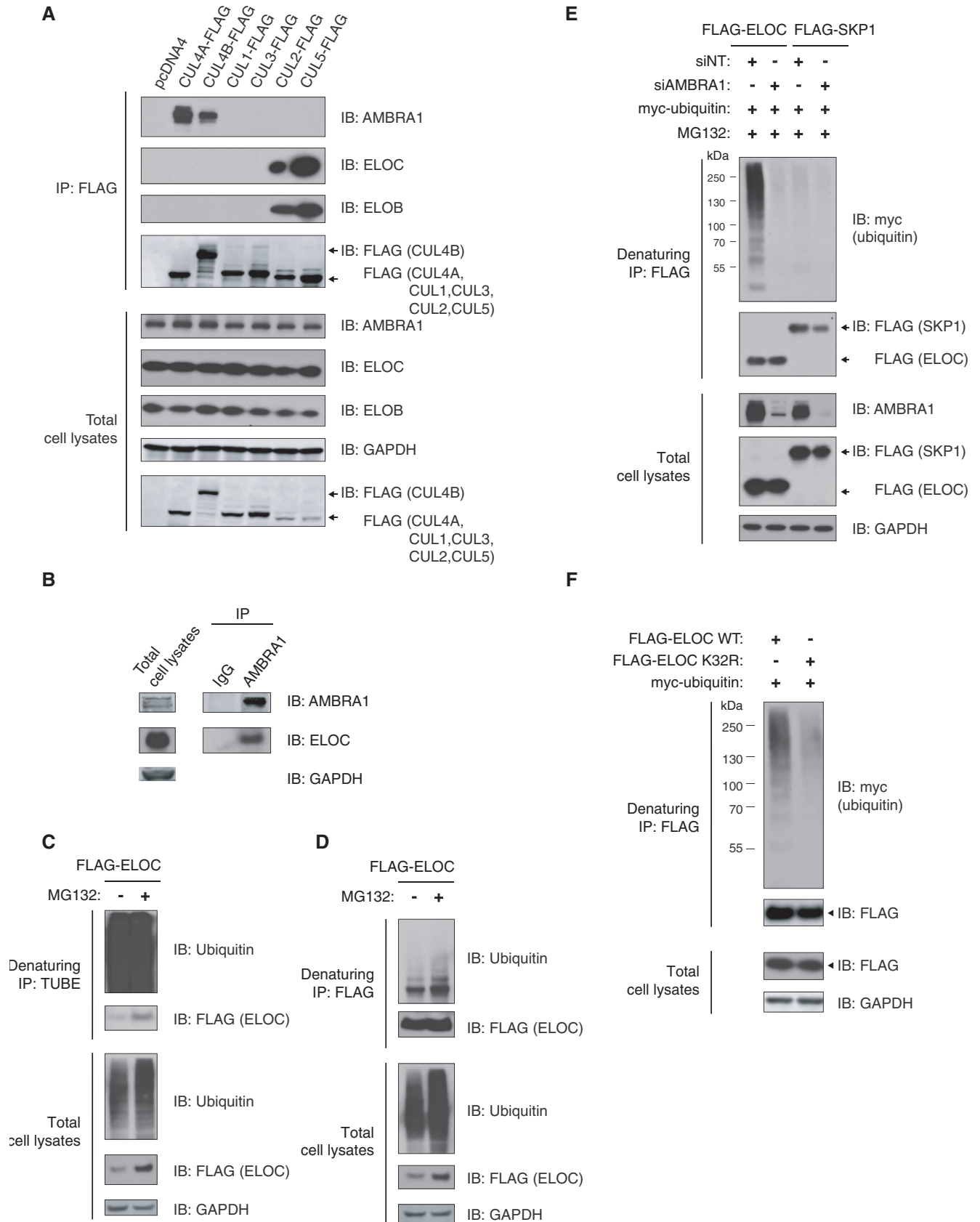


Figure 4.

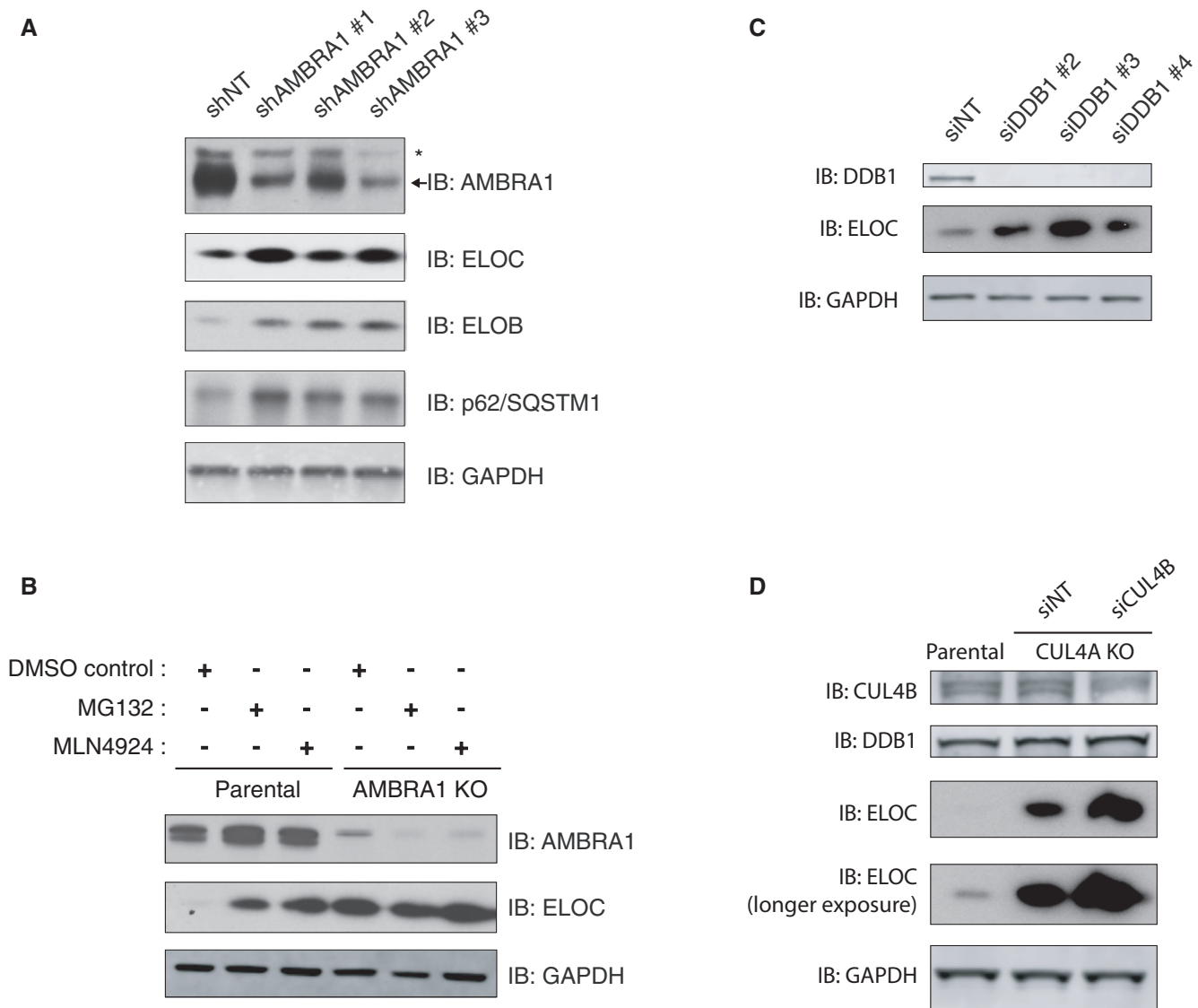


Figure 5. Chemical and genetic perturbation of CRL4^{AMBRA1} increases ELOC protein level.

A Accumulation of ELOC protein in AMBRA1-depleted HEK293T cells. Lysates harvested from HEK293T cells stably expressing non-targeting (NT) or AMBRA1 shRNAs were analyzed by immunoblot. Blot represents three experiments in which stable lines were independently generated. Of note, the sequence of shAMBRA1 #1 corresponds to the sequence of siAMBRA1 used in Fig 4E. Asterisk denotes non-specific bands.

B Inhibition of proteasome and NEDD8-activating enzyme promote ELOC accumulation. Parental or AMBRA1-depleted HEK293T cells were treated with 0.05% DMSO, 5 μ M MG132, or 100 nM MLN4924 for 6 h. Total cell lysates were analyzed by immunoblot.

C DDB1 knockdown increases ELOC protein level. HEK293T cells transfected with 10 nM of NT or DDB1 siRNAs were analyzed by immunoblot.

D CUL4A-depleted HEK293T cells were transfected with 10 nM of NT or CUL4B siRNA and were analyzed by immunoblot.

Source data are available online for this figure.

AMBRA1 regulates CRL5-mediated autocatalytic degradation of SOCS3 and VIF

Next, we evaluated whether AMBRA1 interacts with VIF through ELOC that is assembled into CRL5^{VIF} complexes, and, in a similar manner, whether AMBRA1 interacts with human CRL5 SRs [i.e., suppressors of cytokine signaling proteins (SOCS)]. We affinity-purified FLAG-tagged VIF and SOCS proteins, as well as their respective BC-box mutants (the region through which VIF and SOCS proteins bind to ELOC), from HEK293T cells, and then probed for their

interactions with AMBRA1 by immunoblotting. We found that VIF and several human SOCS proteins co-purified with AMBRA1 (Fig 6A), but the BC-box mutants had significantly decreased interactions with both ELOC and AMBRA1. Furthermore, we showed that knockdown of ELOC decreased VIF and SOCS3 association with AMBRA1 (Fig 6B). These data showed that ELOC mediates the association between AMBRA1 and the VIF/SOCS proteins.

Many SRs of CRL complexes undergo autoubiquitination and autocatalytic degradation, especially in the absence of their substrates (Zhou & Howley, 1998; Galan & Peter, 1999; Wee *et al*,

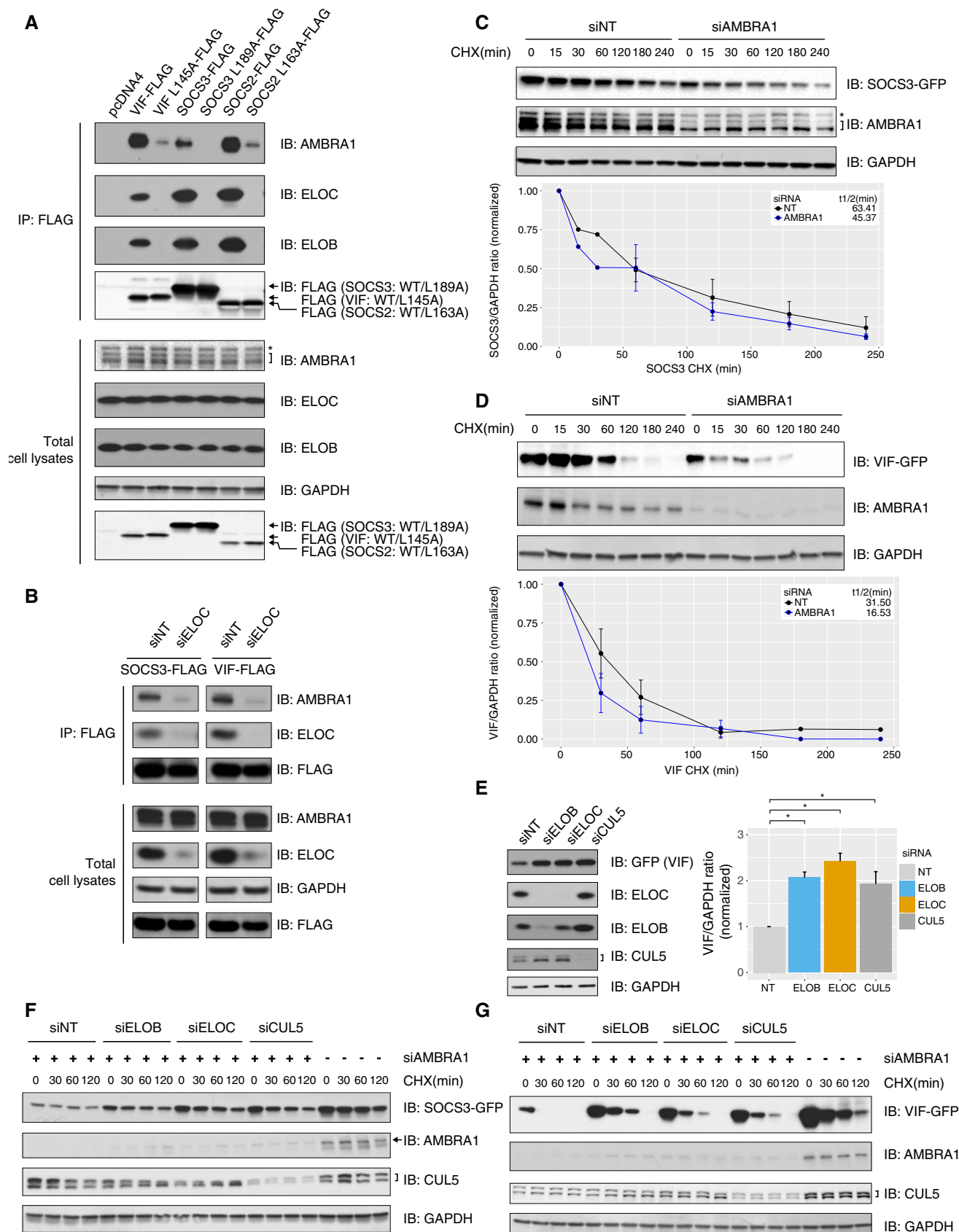


Figure 6.

Figure 6. AMBRA1 regulates CRL5-mediated autocatalytic degradation of SOCS3 and VIF.

- A Mutation of the BC-box disrupts binding of SOCS proteins and VIF to both ELOC and AMBRA1. HEK293T cells transfected with FLAG-tagged VIF, SOCS2, SOCS3, and their respective BC-box point mutants were subjected to affinity purification. IP and input lysates were analyzed by immunoblot. Asterisk denotes non-specific bands.
- B Knockdown of ELOC reduces SOCS3 and VIF binding to AMBRA1. HEK293T cells treated with NT or ELOC siRNA were transfected with FLAG-tagged SOCS3 or VIF, and followed by affinity purification using anti-FLAG beads. IP and input lysates were analyzed by immunoblot.
- C, D AMBRA1 knockdown destabilizes SOCS3 and VIF. HEK293 cells with doxycycline (dox)-inducible SOCS3-GFP (C) or VIF-GFP (D) were transfected with 10 nM of NT or AMBRA1 siRNA for 72–96 h. Protein expression was induced overnight with 1 μg/ml of dox, followed by the addition of 100 μg/ml of CHX at different time points. Lysates were analyzed by immunoblot. Asterisk denotes non-specific bands. Lower panels are densitometric quantification of relative SOCS3 and VIF band intensity (mean ± SEM, *n* = 3). SOCS3 and VIF half-lives were derived from multi-parameter regression using the nplr R package.
- E Inhibiting autocatalysis stabilizes VIF. As described in (C and D), siRNA-treated HEK293 cells with dox-induced VIF-GFP expression were analyzed for VIF steady-state levels by immunoblot. Relative VIF band intensity on immunoblot was quantified and compared by Mann–Whitney–Wilcoxon test (**P* < 0.05). Bar graph represents mean ± SEM, *n* = 3.
- F, G Inhibiting autocatalysis rescues SOCS3 and VIF destabilization when AMBRA1 is depleted. HEK293 cells with dox-inducible SOCS3-GFP and VIF-GFP were co-transfected with 5 nM of AMBRA1 siRNA and 5 nM of NT, ELOB, ELOC, or CUL5 siRNA. Cells were treated with dox and followed by CHX as previously described.

Source data are available online for this figure.

2005; Foe *et al*, 2011). We hypothesized that ELOC accumulation after AMBRA1 knockdown would upregulate CRL5/2 activity and potentially destabilize the SRs via autocatalysis. We assessed the stability of several CRL5/2 SRs in cell lines with AMBRA1 knockdown using CHX (Fig 6C and D for CRL5 SRs; Fig EV5 for CRL2 SRs). Both CRL5 and CRL2 SRs—including SOCS3, VIF, VHL, and PP1L5—were destabilized in AMBRA1-knockdown cells. We also showed that AMBRA1 knockdown reduced the protein half-lives of SOCS3 and VIF by 30% (from 63.41 to 45.37 min) and 50% (from 31.50 to 16.53 min), respectively (Fig 6C and D).

In CRL5-deficient conditions, in which ELOB, ELOC, or CUL5 were knocked down, VIF was stabilized (Fig 6E). VIF was more stable with the L145A mutation, which disrupts CRL5^{VIF} assembly (Fig 6A and Appendix Fig S12; Mehle *et al*, 2004). Importantly, depleting ELOB, ELOC, or CUL5 reversed the decreased SOCS3 and VIF stability following AMBRA1 knockdown (Fig 6F and G). Collectively, these results support the idea that CRL5-mediated autocatalysis destabilizes SRs and highlight the complex dynamics underlying CRL regulation.

CRL4^{AMBRA1} E3 ligase activity negatively regulates the assembly and ubiquitin E3 ligase activity of CRL5 complexes

To learn how AMBRA1 affects SOCS3 and VIF autocatalysis, we evaluated whether AMBRA1's E3 ligase activity targets ELOC to regulate CRL5^{SOCS3} and CRL5^{VIF} complex assembly. We examined the complex assembly through affinity purification of FLAG-tagged SOCS3 and Strep-tagged VIF, and assessed binding of endogenous ELOC, ELOB, and CUL5 by immunoblotting. When WT AMBRA1 was overexpressed, SOCS3 binding to ELOC, ELOB, and CUL5 was

dramatically decreased (Fig 7A, lanes 2,3). Overexpression of ΔH AMBRA1 did not affect SOCS3 binding to ELOB, but it slightly decreased binding to CUL5 (Fig 7A, lanes 4,5). Similarly, WT AMBRA1 disrupted VIF binding to ELOB (Fig 7B, lanes 1,2), which was unaffected by the ΔH mutant and DCAF11, another VIF-interacting DCAF that we previously identified (Fig 7B, lanes 3,4; Fig 1A; Jäger *et al*, 2011a).

To determine whether AMBRA1's disruption of CRL5 complexes compromises ligase activity, we examined SOCS3 and VIF autoubiquitination. Affinity-tagged SOCS3 or VIF was purified under denaturing conditions to assess their covalent modification with myc-ubiquitin in co-expression experiments. We found that overexpression of AMBRA1 reduced SOCS3 autoubiquitination (Fig 7C), as well as VIF autoubiquitination, albeit to a lesser extent (Fig 7D). Of note, CBFβ overexpression reduced VIF autoubiquitination (Fig 7D, lane 4), while CBFβ itself was polyubiquitinated, demonstrating that CBFβ-bound VIF was protected from autoubiquitination (Appendix Fig S13). Conversely, decreased VIF autoubiquitination by AMBRA1 was not a result of a shielding effect, because the ΔH mutant did not reduce VIF autoubiquitination, despite showing slightly higher affinity for VIF (Fig 7D, lanes 2,3; Fig 7B). Collectively, our results indicate that AMBRA1's ubiquitin E3 ligase function is important for downregulating CRL5^{SOCS3} and CRL5^{VIF} complex formation and E3 ligase activity.

CRL4^{AMBRA1} modulates the interleukin-6 (IL-6)/STAT3 pathway regulated by CRL5^{SOCS3}

To evaluate the functional consequences of CRL4^{AMBRA1} downregulating CRL5^{SOCS3}, we examined how AMBRA1 and its E3 ligase

Figure 7. CRL4^{AMBRA1} disrupts the assembly and E3 ligase activity of CRL5^{SOCS3} and CRL5^{VIF} complexes.

- A Disruption of CRL5^{SOCS3} assembly by AMBRA1 WT and not by ΔH mutant overexpression. HEK293T cells stably expressing SOCS3-FLAG were transfected with empty vector, AMBRA1-Strep (2.5 and 5 μg), or AMBRA1-ΔH-Strep (2.5 and 5 μg). Lysates were affinity-purified using anti-FLAG beads to examine SOCS3 binding to CRL5 components. IP and input lysates were analyzed by immunoblot.
- B Disruption of CRL5^{VIF} assembly by AMBRA1 WT and not by ΔH mutant overexpression. HEK293T cells co-expressing VIF-Strep with empty vector, AMBRA1-FLAG, AMBRA1-ΔH-FLAG, or DCAF11-FLAG. Lysates were purified with Strep-Tactin Sepharose beads to examine VIF binding to CRL5 components. IP and input lysates were analyzed by immunoblot.
- C, D Reduction in SOCS3 and VIF autoubiquitination by AMBRA1 WT and not by ΔH mutant overexpression. Similar to (A) and (B), but the cells were co-transfected with myc-ubiquitin and affinity-purified under denaturing conditions with anti-FLAG and Strep-Tactin beads, respectively. IP and input lysates were analyzed by immunoblot. Asterisk denotes non-specific bands.

Source data are available online for this figure.

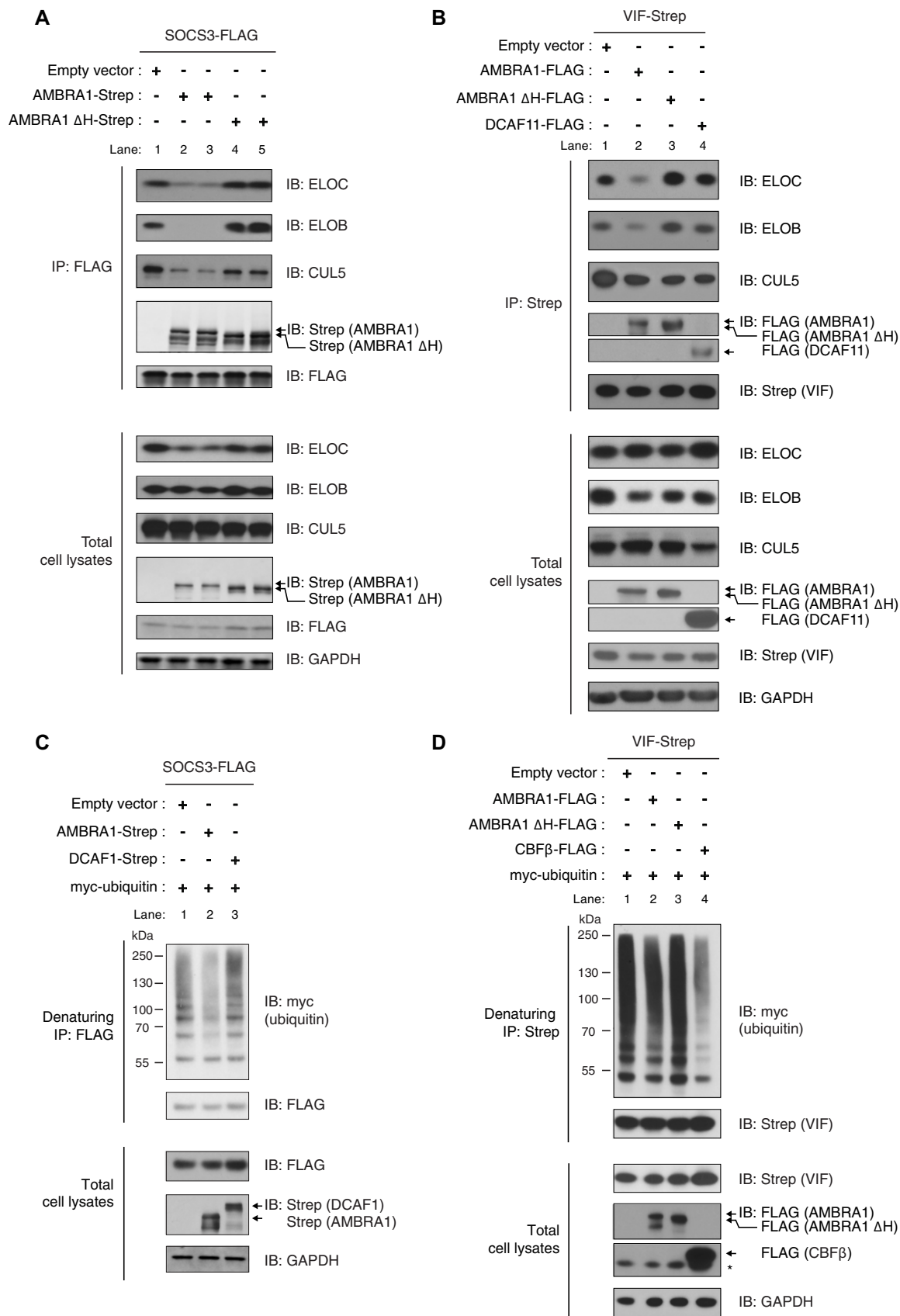


Figure 7.

Figure 8. CRL4^{AMBRA1} negatively regulates CRL5^{SOCS3} to sensitize IL-6-induced STAT3 phosphorylation.

- A AMBRA1 overexpression sensitized IL-6/STAT3 signaling. Hep3B cells stably expressing mCherry-FLAG or AMBRA1-FLAG were serum-starved for 12 h and treated with 20 ng/ml of IL-6 at different time points. Lysates were analyzed by immunoblot.
- B Quantification of pSTAT3/total STAT3 ratios from three independent experiments described in (A) (mean \pm SEM, $n = 3$).
- C Hep3B cells pre-treated with NT or SOCS3 siRNA, stimulated with IL-6, and analyzed by immunoblot.
- D AMBRA1 knockdown blunted IL-6/STAT3 signaling. Hep3B cells stably expressing NT or AMBRA1 shRNA were stimulated with IL-6 and analyzed by immunoblot.
- E Quantification of pSTAT3/total STAT3 ratios from three independent experiments described in (D) (mean \pm SEM, $n = 3$).
- F Knocking down SOCS3 rescued the blunted IL-6/STAT3 response in an AMBRA1-knockdown background. Hep3B cells stably expressing shAMBRA1 #1 were transfected with NT or SOCS3 siRNA, followed by IL-6 treatment.
- G Re-expression of WT AMBRA1, and not the Δ H mutant, rescued the blunted IL-6/STAT3 response in AMBRA1-knockdown background. Hep3B cells stably expressing shAMBRA1 #1 were transduced and selected for AMBRA1 WT or Δ H mutant expression; the established re-expression cell lines were then treated with IL-6 and analyzed by immunoblot.

Source data are available online for this figure.

activity affect interleukin-6 (IL-6)/STAT3 signaling, a pathway regulated by CRL5^{SOCS3}. SOCS3 negatively regulates IL-6-induced STAT3 signaling, and deleting its BC-box prolongs STAT3 phosphorylation (pTyr705 or pSTAT3) due to reduced pSTAT3 suppression by CRL5^{SOCS3} (Crocker *et al*, 2003; Lang *et al*, 2003; Boyle *et al*, 2007). In IL-6 stimulation experiments, human hepatoma Hep3B cells stably expressing mCherry or AMBRA1 were treated with IL-6 at different time points and harvested for immunoblotting. We found that AMBRA1 overexpression sensitized IL-6-induced STAT3 phosphorylation, suggesting that reduced CRL5^{SOCS3} E3 ligase activity weakens pSTAT3 suppression (Fig 8A and B). Also, SOCS3 knockdown phenocopied AMBRA1 overexpression with prolonged STAT3 phosphorylation (Fig 8C). Further, Hep3B cells with AMBRA1 depletion had a blunted response to IL-6-induced STAT3 phosphorylation, supporting that increased CRL5^{SOCS3} activity enhanced pSTAT3 suppression (Fig 8D and E). The response following AMBRA1 knockdown was reversed by concomitant SOCS3 knockdown or re-expression of WT AMBRA1, but not re-expression of the Δ H mutant (Fig 8F and G). These results indicate that CRL4^{AMBRA1} modulates CRL5^{SOCS3} activity to regulate the IL-6/STAT3 pathway.

In summary, we have shown that CRL4^{AMBRA1} targets ELOC, the key adaptor protein in CRL5 and CRL2 complexes, for polyubiquitination and degradation (Fig 9, i), which results in negative regulation of CRL5-complex assembly and activity. We showed that AMBRA1 levels affect the magnitude and kinetic profile of the CRL5^{SOCS3} and CRL5^{VIF} pathways. SOCS3 constitutes an important negative feedback loop for IL-6/STAT3 signaling in which IL-6-induced STAT3 phosphorylation drives expression of SOCS3 and proliferative and inflammatory factors (Fig 9, ii) (Yu *et al*, 2009). CRL5^{SOCS3} dysfunction sensitizes IL6-STAT3 signaling in AMBRA1-overexpressing cells, whereas overly active CRL5^{SOCS3} blunts IL-6-induced STAT3 activation in AMBRA1-depleted cells. Similarly, AMBRA1 knockdown leads to overly active CRL5^{VIF} that confers higher viral infectivity and enhanced A3G degradation by VIF, which is reversed when AMBRA1 expression is restored (Fig 9, iii).

Discussion

Here, we demonstrated that a module shared by a subfamily of CRLs can be ubiquitinated by another CRL E3 ligase to achieve heterologous regulation of the CRL subfamily. We discovered that CRL4^{AMBRA1} targets ELOC, the essential adaptor protein that

mediates the assembly of CRL5/2 complexes, for polyubiquitination and proteasomal degradation. This mechanism supports the notion that crosstalk occurs between CRL4^{AMBRA1} and CRL5 complexes (Jäger *et al*, 2011a; Antonioli *et al*, 2014). We further showed that AMBRA1's E3 ligase function regulates CRL5^{SOCS3} and CRL5^{VIF} complexes and their downstream pathways involving cytokine signaling and viral replication, respectively. Our findings suggest that CRL4^{AMBRA1} controls many CRL5/2 complexes.

CRLs and other ubiquitin E3 ligases undergo complex regulatory processes, including autocatalysis, heterologous ubiquitination by other E3 ligases, and other mechanisms targeting different moieties of the E3 complex (Petroski & Deshaies, 2005; Weissman *et al*, 2011). When these ligases are overly active, SRs of CRL1, CRL3, and CRL4 are prone to autocatalytic degradation (Zhou & Howley, 1998; Geyer *et al*, 2003; Fischer *et al*, 2011). Conversely, SRs of CRL2 and CRL5, except for VHL and VIF, have not been well-studied for their autocatalytic activities (Lisztwan *et al*, 1999; Mehle *et al*, 2004). Here, we showed that SOCS3 and VIF, SRs of CRL5, are autoubiquitinated, and their protein levels are regulated by autocatalysis.

To examine the effect of a CRL regulator on the target CRLs, researchers have commonly assessed SR stability. For example, many CRL1 SRs are destabilized in a COP9 signalosome (CSN)-defective background as a result of CRL1 hyperactivation (Schmidt *et al*, 2009). Additionally, depleting glomulin, an RBX1-binding protein that negatively regulates RBX1-containing CRL complexes, causes hyperactivation of the complexes, destabilizing the CRL1 SR FBW7, RBX1, and RBX1-bound cullins (Duda *et al*, 2012; Tron *et al*, 2012). Hyperactivation of CRL1^{FBW7} is associated with accumulation of its substrates cyclin E and c-Myc due to premature destruction of FBW7 and the rest of the complex. Here, we discovered that AMBRA1 depletion hyperactivates CRL5 to similarly destabilize SOCS3 and VIF (Fig 6). Surprisingly, elevated CRL5^{SOCS3} and CRL5^{VIF} activities positively correlated with the ligase-regulated functions and increased substrate clearance (Figs 8, 2 and EV3). We reasoned that CRL5^{SOCS3} and CRL5^{VIF} complexes may predominantly contain SR-substrate heterodimers instead of monomers, whereas CRL1^{FBW7} assembly and autocatalysis likely precede substrate recruitment (Koepp *et al*, 2001; Welcker *et al*, 2013). Consistent with this notion, suppressing SR autocatalytic degradation in the presence of its substrate (i.e., the substrate-shielding effect) occurs in CRL complexes (de Bie & Ciechanover, 2011; Foe *et al*, 2011).

CRL master regulators (e.g., CSN, CAND1, glomulin) control the assembly and disassembly of CRL complexes on a global level,

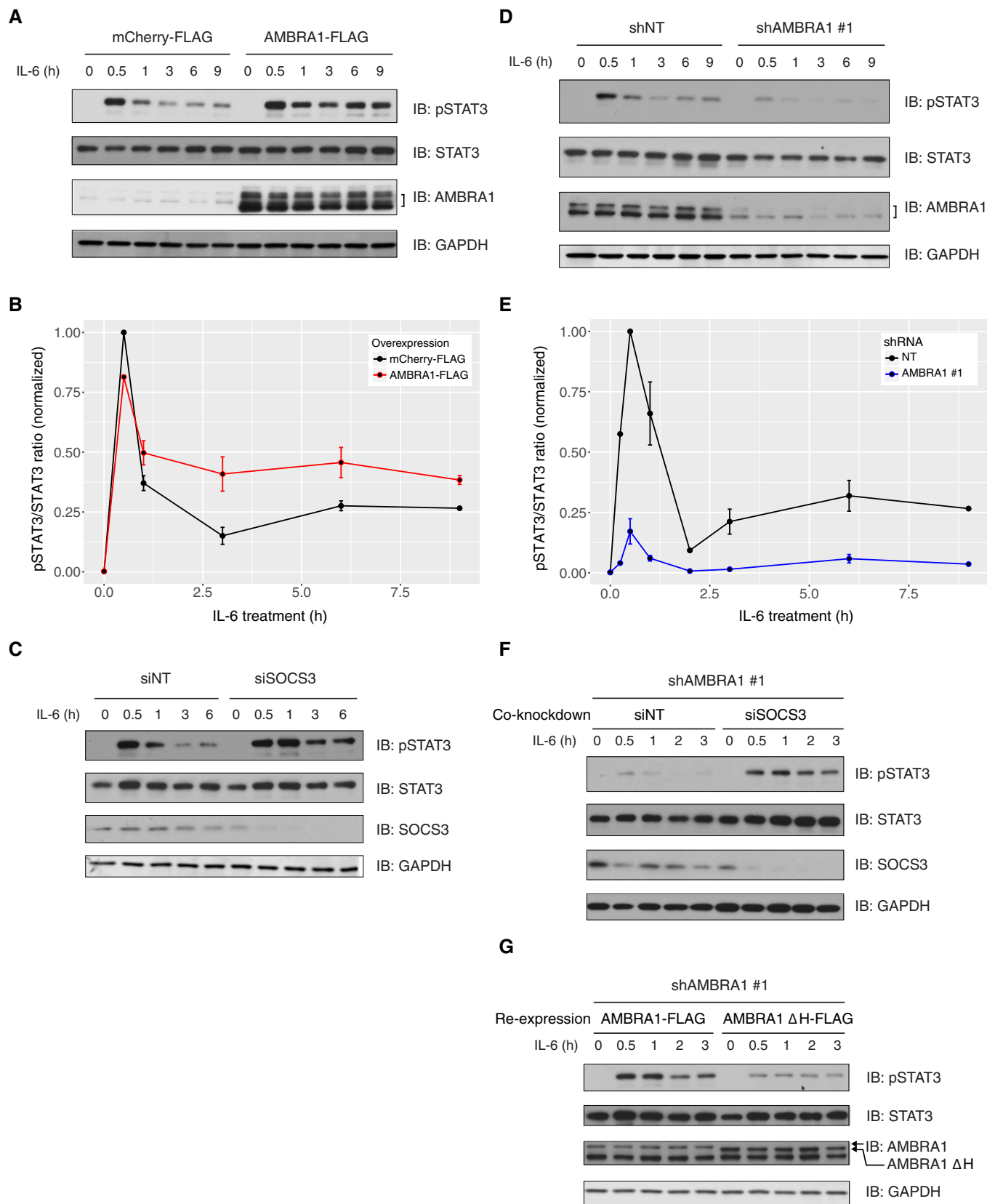


Figure 8.

(i) CRL4^{AMBRA1} targets ELOC for polyubiquitination and degradation

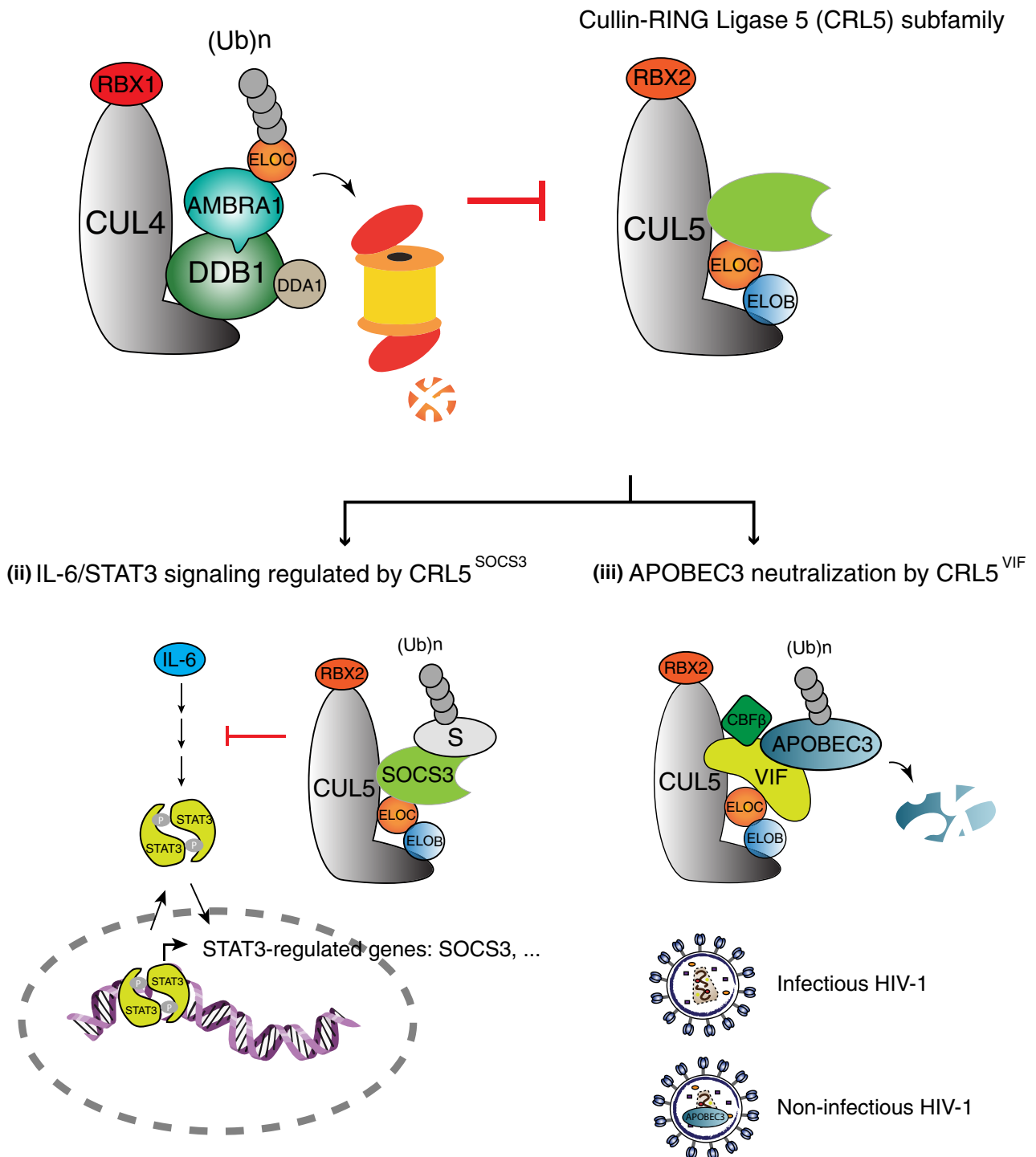


Figure 9. Proposed model depicting how CRL4^{AMBRA1} regulates CRL5 complexes to modulate CRL5-regulated pathways.

CRL4^{AMBRA1} targets ELOC for polyubiquitination and degradation (i), and thereby negatively regulates the assembly and ubiquitin E3 ligase activity of CRL5 complexes. AMBRA1 and its E3 ligase function (as demonstrated by the ΔH mutant's loss of function) modulate the responses of IL-6/STAT3 signaling. S denotes an unknown substrate. (ii) and APOBEC3 degradation (iii), which are regulated by CRL5^{SOCS3} and CRL5^{VIF} complexes.

whereas heterologous CRL regulation can target a specific CRL complex (e.g., CRL4^{CDT2} disruption by CRL1^{FBXO11} via CDT2 degradation; Abbas *et al*, 2013; Rossi *et al*, 2013). Interestingly, regulation of the CRL5 subfamily by CRL4^{AMBRA1} falls in the middle of the CRL regulatory spectrum. Dynamic CRL-complex assembly ensures timely substrate degradation in response to environmental cues. CAND1, as an exchange factor, promotes the dissociation between cullins and SR-adaptor dimers after the cullins are de-NEDDylated by CSN. This dissociation is followed by the assembly of adaptor-free cullins and new SR-adaptor dimers, shaping the repertoire of CRL complexes (Bennett *et al*, 2010; Pierce *et al*, 2013). In contrast to CAND1, the CRL4^{AMBRA1} ubiquitin E3 ligase requires ligase activity to promote disassembly of target CRLs. In theory, CRL4^{AMBRA1} can act on both cullin-bound and cullin-free ELOC. We showed that CRL4^{AMBRA1} targets the cullin-bound ELOC to attenuate CRL5 activity. However, we do not know whether CRL4^{AMBRA1} also targets a pool of cullin-free SR-adaptor dimers. Of note, SRs and their associated adaptors form strong subcomplexes before encountering the cullins (Babon *et al*, 2009). Thus, CRL4^{AMBRA1} may remodel SR-adaptor dimers via ELOC degradation, thereby affecting the landscape of CRL5 complexes.

We found that CRL4^{AMBRA1} mediates ELOC polyubiquitination and degradation, which is required for AMBRA1's effect on CRL5 disassembly. Our findings have extended our understanding of how CRL5 complexes are regulated by AMBRA1. Previous work by Antonioli *et al* (2014) showed that increased AMBRA1 level sequestered ELOB and inhibited CRL5-mediated DEPTOR degradation. Here, we found that overexpression of the ΔH mutant, which retains ELOC interaction, was insufficient to disrupt CRL5 complexes and to downregulate CRL5 activity (Fig 7A, B and D). These data support the notion that CRL5 regulation by AMBRA1 requires the ubiquitin E3 ligase function of AMBRA1. Interestingly, starvation-induced autophagy regulates AMBRA1 autocatalysis by promoting CRL4^{AMBRA1} assembly (Antonioli *et al*, 2014). However, binding of ELOC to AMBRA1 would theoretically stabilize AMBRA1 by blocking its autocatalysis. It requires further study to understand the sequence of events upon autophagy activation, including CRL4^{AMBRA1} activation/inactivation and how it coordinates with other ubiquitin E3 ligases to regulate the autophagy response (Xia *et al*, 2013, 2014). Despite the connection between AMBRA1 and autophagy, our study focused on the role of CRL4^{AMBRA1} in regulating human SOCS proteins and HIV-1 VIF.

We showed that CRL4^{AMBRA1} modulates the amplitude and duration of IL-6-induced STAT3 activation by regulating CRL5^{SOCS3}. Similarly, it regulates CRL5^{VIF}-mediated A3G degradation and HIV-1 infectivity. Thus, by blocking inhibitory events, we may fine-tune substrate stability and precisely regulate signaling kinetics and intensity to control time-sensitive cellular processes. Our knowledge of such regulation was limited to cell cycle progression (Abbas *et al*, 2013; Rossi *et al*, 2013). Here, we reason that a similar mechanism for CRL5 regulation by CRL4^{AMBRA1} is important for cytokine signaling and viral replication with respect to modulating the output of STAT3 phosphorylation and the level of the antiviral DNA-editing enzyme A3G. SOCS3 requires its E3 ligase function to fully suppress STAT3 signaling (Boyle *et al*, 2007). Although the identity of CRL5^{SOCS3} substrates *in vivo* remains poorly defined, reconstituted CRL5^{SOCS3} complex ubiquitinates the IL-6/STAT3 signaling transducers JAK2 and gp130 *in vitro* (Kershaw *et al*, 2014). IL-6/STAT3

signaling strongly interacts with pro-inflammatory pathways to govern diverse immune responses. SOCS3 controls timely termination of STAT3 activation, and prolonged activation of STAT3 or SOCS3 dysfunction has been linked to aberrant T-cell development, tumorigenesis, and other malignancies (Yoshimura *et al*, 2007; Yu *et al*, 2009). Further work is needed to understand these functional implications when CRL4^{AMBRA1} downregulates CRL5^{SOCS3}.

Our work also provides a new axis of CRL5^{VIF} regulation. Researchers are working to find small molecules that inhibit CRL5^{VIF}-mediated A3G degradation (Nathans *et al*, 2008). The effectiveness of this process can be limited by virally adapting the VIF-A3G interaction, rendering delayed replication kinetics rather than complete elimination of viral replication (Richards *et al*, 2015). However, we need to better understand how CRL4^{AMBRA1} controls CRL5^{VIF} activity to affect HIV-1 replication kinetics, and whether CRL4^{AMBRA1} function is affected during viral infection and in different cytokine contexts.

In summary, our study reveals how the modularity of multi-subunit CRLs in human cells specifically regulates a subclass of CRL family members. This finding unveils a new trajectory for exploring how CRL4^{AMBRA1} regulates a network of cytokine suppressors and viral factors that require their CRL5 ligase function to counteract overshooting cytokine responses and to promote viral pathogenesis (Zhang *et al*, 2001; Boyle *et al*, 2007; Pozzebon *et al*, 2013; Kane *et al*, 2015).

Materials and Methods

Cell culture and generation of stable cell lines with cDNA or shRNA expression

HEK293T and HEK293 cells were obtained from the UCSF Cell Culture Facility (CCF). HEK293T cells were maintained in high-glucose DMEM supplemented with 10% fetal bovine serum (FBS; Gibco), 1 mM sodium pyruvate (Na-Py), and 1% penicillin/streptomycin (Pen/Strep). HEK293 cells were cultured in MEM with Earle's salts containing 10% FBS, 1 mM Na-Py, 2 mM L-glutamine, and 1% Pen/Strep. Hep3B cells were obtained from Dr. Rik Derynck's laboratory (UCSF). Stable cell lines with cDNA or shRNA expression were generated by lentivirus transduction followed by antibiotics selection at an optimal concentration as determined by a kill curve, or alternatively followed by FACS (fluorescence-activated cell sorting) based on fluorescent protein expression with the lentiviral vectors used. Lentiviruses were prepared per the manufacturers' protocols, and were concentrated with 8.5% of PEG-6000 and 0.3 M of NaCl and resuspended in culture media or PBS.

Recombinant DNA constructs

DNA expression constructs were prepared by standard molecular cloning and sequence verified. Mutants of VIF/SOCS expression constructs and shRNA-resistant AMBRA1 constructs were generated by site-directed mutagenesis in the pcDNA4/TO vector using Pfu Turbo DNA polymerase (Agilent) and subcloned into lentiviral vectors when needed. All HIV-1 recombinant DNA (rDNA) constructs used in this study were described previously (Jäger *et al*,

2011a). The sequence information for human rDNAs includes the following: AMBRA1 (NM_017749.3), DCAF1 (NM_014703.2), ELOC (NM_005648.3), ELOB (NM_007108.3), SKP1 (NM_170679.2), SOCS3 (NM_003955.4), SOCS2 (NM_003877.4), VHL (NM_000551.3), PPL5/LRR1 (NM_152329.3), and CBF β (NM_001755.2). See Appendix Table S1 for the list of DNA constructs and the associated vectors.

Human T-cell isolation and culture

Whole blood was collected from healthy human donors with approval from the UCSF Committee on Human Research. CD4⁺ T cells were isolated from blood within 12 h of blood collection using SepMate tubes and the EasySep Human CD4⁺ T-cell Enrichment Kit, according to manufacturer instructions (STEMCELL Technologies). Isolated CD4⁺ T cells were suspended in complete RPMI consisting of RPMI-1640 (Sigma) supplemented with 5 mM HEPES (UCSF CCF), 2 mM L-glutamine (UCSF CCF), 50 μ g/ml Pen/Strep (UCSF CCF), and 10% FBS (Sigma). Upon isolation, cells were immediately stimulated on anti-CD3 (Tonbo, clone UCHT1)-coated plates in the presence of soluble 5 μ g/ml anti-CD28 (Tonbo, clone CD28.2) and 20 U/ml IL-2. Cells were cultured for 3 days prior to electroporation.

Cas9 RNP generation and electroporation

Cas9 ribonucleoproteins (RNPs) were generated and electroporated into cells using the Amaxa P3 Primary Cell 96-well Nucleofector Kit and 4D-Nucleofector (Lonza) to mediate knockout. Briefly, crRNAs specific to AMBRA1 or control genes crRNAs (Dharmacon) were resuspended at 160 μ M and mixed with an equal volume of 160 μ M tracrRNA (Dharmacon). Incubation for 30 min at 37°C yielded gRNA at 80 μ M that was, in turn, incubated with an equal volume of 40 μ M Cas9-NLS (MacroLab, UC Berkeley) for 15 min at 37°C to yield RNPs at a final concentration of 20 μ M. RNPs were stored in 3.5 μ l aliquots at -80°C until use. See Appendix Table S2 for the list of guide RNAs used in Cas9 RNP preparation and HIV-1 infection.

For each editing reaction, approximately 4–5 \times 10⁵ stimulated T cells were suspended in 20 μ l P3 buffer. These cells were then mixed with thawed RNPs, and the resulting mixture was transferred to a 96-well reaction cuvette. Cells were electroporated using program EH-115. Immediately after editing, 80 μ l pre-warmed, complete RPMI was added to each well, and cells were allowed to recover for 30 min at 37°C. Cells were then moved to 96-well flat-bottomed plates, re-stimulated with anti-CD3/anti-CD2/anti-CD28 beads (T-Cell Activation/Expansion Kit; Miltenyi Biotec) in a total volume of 200 μ l, and cultured for 6 days in the presence of 20 U/ml IL-2. On Day 6, cells were replica-plated into plates for infection in technical triplicate, roughly 50,000 cells per well in 200 μ l media. At the same time, protein extracts from each cell pool were prepared in Laemmli sample buffer for immunoblot verification of gene product perturbation.

HIV-1 infection and analysis

For primary T-cell infection experiments, stocks of HIV-1 NL4-3 with an IRES-GFP reporter immediately following the *nef* open

reading frame were generated as previously described (Hultquist *et al*, 2016). Then, 24 h after replica plating, 2 μ l (1% of total volume) of concentrated virus was directly added to culture media in technical triplicate. Time points were taken at days 3, 5, and 7, or as otherwise indicated, by cell resuspension, removal of 35% of the culture by volume, and fixation in a final concentration of 1% formaldehyde. On days 3 and 5, the removed volume was replaced with complete RPMI plus 20 U/ml IL-2. Percent live and percent GFP⁺ cells were monitored by flow cytometry on an Attune NxT Flow Cytometer with HTS (Life Technologies) with detection of LightScatter, GFP, and AmCyan and Pacific Blue for autofluorescence correction. Analysis of flow data was performed with FlowJo v9.3.2 (TreeStar), and data processing was done in R (Team, 2015). For infection experiments in SupT11-APOBEC3G cells, we infected the cells with Vsvg-pseudotyped HIV-1 NL4-3 that either carries IRES-GFP reporter downstream of *nef* or Gag-GFP fusion reporter (Muller *et al*, 2004). Cells were incubated with viral particles at 37°C for an hour and then were spun at 300 \times g for 10 min. After removal of supernatant and resuspended in fresh media, the cells were cultured for 48 h and then were fixed by 1% paraformaldehyde/PBS followed by flow cytometry analysis.

Transfection of DNA plasmids and siRNAs

DNA plasmids used in mammalian cell transfections were prepared with NucleoBond Xtra Midi EF (Macherey–Nagel) and quantified with a NanoDrop One UV-Vis spectrophotometer (Thermo Scientific). Plasmids were transfected in HEK293T cells using PolyJet (SigmaGen), and cells were harvested 24–48 h post-transfection. Dried siRNAs were resuspended in 1 \times siRNA buffer (Dharmacon), aliquoted, and stored at -80°C. HEK293T and HEK293 cells were seeded at 4–5 \times 10⁵ per well in a 6-well format (Corning Costar) and transfected with 10 nM siRNA ~6 h post-seeding using RNAiMAX (Thermo Scientific); cells were split to 12-well plates 3–4 days post-transfection for downstream experiments (cells were exposed to siRNA for a minimum of 6 days before harvested for analysis). For DDB1 and CUL4B knockdown, cells were transfected again with 10 nM siRNA after splitting and were collected for analysis after a total of 7-day siRNA treatment. Hep3B cells were seeded at 3 \times 10⁵ per 60-mm dishes and transfected with 5–10 nM siRNA using DharmaFECT 4 (Dharmacon) shortly after seeding; culture media were replaced with fresh media ~4 h post-transfection. See Appendix Table S3 for siRNA and shRNA sequences.

Generation of AMBRA1-knockout and ATG-knockout cell lines

HEK293T cells with AMBRA1 knockout were generated by transient transfection of all-in-one SpCas9-P2A-GFP (Addgene #48138) encoding U6-driven expression of AMBRA1 sgRNA; cells were sorted 48–72 h post-transfection based on GFP expression. HEK293T cells with ATG7 and ATG12 knockout were generated by transient transfection of SpCas9-P2A-puro (Addgene #48139) encoding U6-driven expression of sgRNA targeting ATG7 and ATG12; cells were selected 48–72 h post-transfection using 1 μ g/ml puromycin (Sigma-Aldrich) for 48 h. For DNA analysis, genomic DNA samples were prepared using QuickExtract (Epicentre) supplemented with RNase and proteinase K. Polyclonal knockout populations were collected for Surveyor (IDT), TIDE (Brinkman *et al*, 2014), and immunoblotting.

Single-sorted knockout cells were expanded/banked and confirmed by genotyping and immunoblotting. For genotyping, we PCR amplify the edited regions from the genomic DNA extracted from individual knockout clonal cells, followed by standard molecular cloning procedure and Sanger sequencing to confirm insertion/deletion. See Appendix Table S3 for sgRNA sequences.

Generation of CUL4A-knockout cell lines

HEK293T cells were seeded at 5×10^5 cells per well in a 6-well format and transfected with 0.5 μ g px330-CUL4A-exon1 plasmid (containing Cas9 and CUL4A sgRNA, targeting exon 1: 5'-CGGCGTTCCGG CCCAGCC-3'; Cong *et al.*, 2013). After 3 days, cells were seeded and transfected again, this step was repeated two times for a total of three rounds of transfections with px330-CUL4A-exon1. Subsequently, cells were collected, serially diluted to 30 cells/ml and seeded into 96-well plates with < 1 cell/well. After 7 days, single-cell clones were selected and transferred to 24-well plates and genomic DNA was collected (Epicentre QuickExtract) for screening via PCR. Deletion of a region surrounding the start codon of CUL4A on Chromosome 13 was confirmed via genomic PCR using the Fwd 3'-GAGGGGGTGTCCGAATCTCT-5' and Rev 3'-TCACCTGGTAGAG CTCCTCG-5' primer pair. Loss of CUL4A protein was confirmed via immunoblot.

Cell lysis and immunoblotting

For IP Western blotting, CHX, and other standard assays, cells were lysed in 1 \times RIPA buffer containing 50 mM Tris-HCl, pH 7.5, 150 mM NaCl, 1% NP-40, 0.5% sodium deoxycholate, 0.1% SDS, 1 \times protease-inhibitor cocktail (Roche), and 1 \times phosphatase-inhibitor cocktail (Roche). Lysates were quantified with a BCA assay (Bio-Rad); samples were prepared in 1 \times LDS sample buffer supplemented with 1 \times TCEP solution (Thermo), boiled for 5 min, and separated by SDS-PAGE (NuPAGE gels with MES/SDS buffer, Thermo; Criterion Tris-HCl gels with Tris/glycine/SDS buffer, Bio-Rad). Gels were stacked with 0.22- μ m activated PVDF membranes and filter papers following standard wet-blotting procedures using Mini Trans-Blot Cell or Criterion Blotter (Bio-Rad). See Appendix Table S4 for the list of antibodies used in this study.

IL-6 stimulation and cell lysate preparation

For IL-6 stimulation assays, Hep3B cells were serum-starved for 12 h and treated with 20 ng/ml IL-6 (EMD-Millipore; freshly diluted in serum-free media) for the indicated times. Cells were washed once with DPBS, snap-frozen on dry ice, and lysed in modified RIPA buffer containing 50 mM HEPES, pH 7.4, 150 mM NaCl, 10% glycerol, 1% Triton X-100, 1% sodium deoxycholate, 0.1% SDS, 1.5 mM MgCl₂, 1 mM EGTA, 100 mM NaF, 1 mM PMSF, 10 μ g/ml leupeptin, 1 mM Na₃VO₄, and 10 mM Na₄P₂O₇. Lysates were quantified and analyzed by immunoblotting as described.

Affinity purification, mass spectrometry, and data analysis

Affinity purification was performed as previously described with some modifications (Jäger *et al.*, 2011a). Briefly, FLAG-tagged AMBRA1 was transiently expressed in HEK293T and followed

by cell lysis and purification using anti-FLAG M2 beads (Sigma-Aldrich). Beads were then washed three times with IP buffer (50 mM Tris-HCl pH 7.5, 150 mM NaCl, and 1 mM EDTA) containing 0.05% NP-40, followed by an additional wash with IP buffer to remove detergents. The immunoprecipitates were eluted in IP buffer containing 100 μ g/ml of 3 \times FLAG peptides (MS-grade, Elimbio) and 0.05% RapiGest SF surfactant (Waters). Purified protein eluates were digested with trypsin for LC-MS/MS analysis. Samples were denatured and reduced in 2 M urea, 10 mM NH₄HCO₃, and 2 mM DTT for 30 min at 60°C, then alkylated with 2 mM iodoacetamide for 45 min at room temperature. Trypsin (Promega) was added at a 1:100 enzyme:substrate ratio and digested overnight at 37°C. Following digestion, samples were concentrated using C18 ZipTips (Millipore) according to the manufacturer's specifications. Digested peptide mixtures were analyzed by LC-MS/MS on a Thermo Scientific Velos Pro system equipped with a Proxeon Easy nLC high-pressure liquid chromatography and autosampler system. Samples were injected onto a pre-column (2 cm \times 100 μ m I.D. packed with ReproSil Pur C18 AQ 5 μ m particles) in 0.1% formic acid and then separated with a 2-h gradient from 5 to 30% ACN in 0.1% formic acid on an analytical column (10 cm \times 75 μ m I.D. packed with ReproSil Pur C18 AQ 3 μ m particles). The mass spectrometer collected data in a data-dependent fashion, collecting one full scan followed by 20 collision-induced dissociation MS/MS scans of the 20 most intense peaks from the full scan. Dynamic exclusion was enabled for 30 s with a repeat count of 1. The raw data were matched to protein sequences by the Protein Prospector algorithm. Data were searched against a database containing SwissProt Human protein sequences (downloaded on March 6, 2012) and concatenated to a decoy database in which each sequence was randomized to estimate the false-positive rate. The searches considered a precursor mass tolerance of 1 Da and fragment ion tolerance of 0.8 Da, and considered variable modifications for protein N-terminal acetylation, protein N-terminal acetylation and oxidation, glutamine-to-pyroglytamate conversion for peptide N-terminal glutamine residues, protein N-terminal methionine loss, protein N-terminal acetylation and methionine loss, methionine oxidation, and constant modification for carbamidomethyl cysteine. Prospector data were filtered using a maximum protein expectation value of 0.01 and a maximum peptide expectation value of 0.05. AMBRA1 interactors were scored by Comparative Proteomic Analysis Software Suite (CompPASS; Sowa *et al.*, 2009). Protein network data visualization was implemented in Cytoscape (Shannon *et al.*, 2003).

Comparative proteomics data acquisition and analysis

Digested peptide mixtures derived from affinity purifications were analyzed by LC-MS/MS on a Thermo Scientific Orbitrap Fusion mass spectrometry system equipped with a Proxeon Easy nLC 1,000 ultra-high-pressure liquid chromatography and autosampler system. Samples were injected onto a C18 column (25 cm \times 75 μ m I.D. packed with ReproSil Pur C18 AQ 1.9 μ m particles) in 0.1% formic acid and then separated with a 60-min gradient from 5 to 30% ACN in 0.1% formic acid at a flow rate of 300 nl/min. The mass spectrometer collected data in a data-dependent fashion, collecting one full scan in the Orbitrap at 120,000 resolution followed by 20 collision-induced dissociation MS/MS scans in the dual linear ion trap for the 20 most intense peaks from the full scan. Dynamic exclusion

was enabled for 30 s with a repeat count of 1. Charge state screening was employed to reject analysis of singly charged species or species for which a charge could not be assigned.

Raw data were analyzed using the MaxQuant algorithm (version 1.5.2.8; Cox & Mann, 2008) for the identification and quantification of peptides and proteins. Data were searched against a database containing SwissProt Human (downloaded 12/2014) and concatenated to a decoy database in which each sequence was randomized to estimate the false discovery rate (FDR). Variable modifications were allowed for methionine oxidation and protein N-terminus acetylation. A fixed modification was indicated for cysteine carbamidomethylation. Full trypsin specificity was required. The first search was performed with a mass accuracy of ± 20 parts per million, and the main search was performed with a mass accuracy of ± 4.5 parts per million. A maximum of five modifications and two missed cleavages were allowed per peptide. The maximum charge was set to 7+. Individual peptide mass tolerances were allowed. For MS/MS matching, the mass tolerance was set to 0.8 Da and the top 8 peaks per 100 Da were analyzed. MS/MS matching was allowed for higher charge states, and water and ammonia loss events. The data were filtered to obtain a peptide, protein, and site-level false discovery rate of 0.01. The minimum peptide length was 7 amino acids. Results were matched between runs with a time window of 2 min for biological replicates. Subsequently, SAINTexpress (Significance Analysis of INteractome) was applied to score protein networks components of AMBRA1 and its mutants (Teo *et al.*, 2014) by comparing spectral counts of identified proteins for AMBRA1 WT and its mutants to a vector control. To discriminate bona fide protein interactors of AMBRA1 WT and mutants from background proteins, we set a FDR threshold of 0.05. To generate an overall list of AMBRA1 interactors, we combined the proteins with an FDR below 0.05 for AMBRA1 WT and mutants. To compare abundance of the specific AMBRA1 interactors between WT and mutants AMBRA1, statistical analysis of the data was performed using the statistical models implemented in the MSstats package to calculate fold changes (FC) and adjusted *P*-values (Choi *et al.*, 2014). To reduce variation between AMBRA1 constructs and their biological replicates, we performed a constant normalization based on the median protein intensities per MS run. Proteins with an adjusted *P* ≤ 0.05 and a FC ≥ 1.5 were considered significant.

Tandem affinity purification

HEK293T cells co-expressing Strep-tagged and FLAG-tagged bait proteins were purified in two steps. Cells were lysed in 50 mM Tris-HCl pH 7.5, 150 mM NaCl, and 1 mM EDTA (IP buffer) containing 0.5% NP-40 and 0.25% CHAPS on a tube rotator at 4°C for 30 min. The cleared lysates were collected after centrifugation and purified with Strep-Tactin beads for at least 2 h at 4°C. Beads were washed three times with IP buffer containing 0.05% NP-40 and eluted with 1× D-Desthiobiotin buffer (IBA). The eluates were immunoprecipitated with anti-FLAG M2 beads (Sigma-Aldrich) for at least 2 h at 4°C. Beads were then washed three times with IP buffer containing 0.05% NP-40, followed by an additional wash with IP buffer to remove detergents. The immunoprecipitates were eluted in IP buffer containing 100 µg/ml of 3× FLAG peptides (MS-grade, Elim Biopharmaceuticals) and 0.05% RapiGest SF surfactant (Waters).

Cell-based ubiquitination assay

HEK293T cells were pelleted and heat-denatured in 50 mM Tris-HCl pH 7.5, 1% SDS, and 5 mM DTT containing 5 µg/ml DUB inhibitor PR-619 (LifeSensors). Cell lysates were diluted 10-fold to reduce the concentration of SDS and pre-cleared using Sepharose beads, and the supernatants were collected for IP. After overnight incubation with anti-FLAG M2 (Sigma-Aldrich), Strep-Tactin beads (IBA), or anti-ubiquitin TUBE1 agarose (LifeSensors), the beads were washed three times with 50 mM Tris-HCl pH 7.5, 500 mM NaCl, 1 mM EDTA, 0.5% NP-40, 10% glycerol, 1 mM 2-mercaptoethanol, and a cocktail of protease inhibitors (Roche). The affinity-tagged proteins were eluted with 250 µg/ml of 3× FLAG peptides (Sigma-Aldrich) or 1× D-Desthiobiotin buffer (IBA).

Quantification of Western blot band intensity and statistical analysis

Densitometric quantification of band intensity on immunoblots was carried out by Image Studio Lite software (LI-COR). Mann-Whitney-Wilcoxon test was implemented in R (Team RC, 2015) using plyr package with the wilcox.test() function. Volcano plots for visualizing comparative proteomics were generated by R, plotting statistical significance ($-\text{Log}_{10}$ transformed) versus fold change (Log_2 transformed). For the calculations of protein half-lives, we use the R package nplr (n parameter logistic regression).

Quantitative real-time PCR measurements of mRNA expression

Total RNA was extracted using RNeasy extraction kit (Qiagen), followed by cDNA synthesis using the one-step iScript cDNA synthesis kit (Bio-Rad). Quantitative real-time PCR (qPCR) was performed on cDNA samples using iQ SYBR Green supermix (Bio-Rad) and measured by CFX96 touch real-time PCR system (Bio-Rad). mRNA expression levels were initially expressed as $2^{\Delta\text{Ct}}$, in which ΔCt represents the difference in average Ct derived from triplicate measurements comparing mRNA of interest and the internal control ribosomal protein *L19* mRNA. The measurements were then normalized against *GAPDH* mRNA expression and plotted in ratio relative to the shNT samples. Primers for qPCR were pre-designed (IDT) or otherwise indicated: *AMBRA1* (Hs.PT.58.51492), *ELOB* (Hs.PT.58.38397524), *ELOC* (Hs.PT.58.15710426), *GAPDH* (Hs.PT.39a.22214836), and *L19* (TCGCCTCTAGTGCTCTCCG).

Subcellular fractionation

Cytoplasmic and nuclear fractionation was carried out as previously described (Du *et al.*, 2017). HEK293T cells were treated with CHX for the indicated time and harvested by centrifugation. The cell pellets were lysed in NE-PER Nuclear and Cytoplasmic Extraction reagents (Thermo Scientific) following the manufacturer's instructions. The purity of fractionated samples was examined by immunoblot using *GAPDH* and histone H3 as cytoplasmic and nuclear markers, respectively.

Expanded View for this article is available online.

Acknowledgements

We thank members of the Krogan laboratory for helpful discussion, especially Priya Shah, Manon Eckhardt, and Joshua Kane. Special thanks to Crystal Herron for manuscript editing and Mike Shales for help with figure layout and presentation. We also thank John Von Dollen and Erik Verschueren for technical assistance with implementing MS-scoring algorithms in R environment; Sourav Bandyopadhyay (UCSF) for providing plasmids of SOCS2, SOCS3, VHL, and PP1L5; Rik Derynck (UCSF) for providing Hep3B cells; Reuben Harris (University of Minnesota) for providing SupT11-APOBEC3G cell line; and Feng Zhang (MIT) for gifting pSpCas9(BB)-2A-GFP (PX458; Addgene plasmid # 48138). The mass spectrometry proteomics data have been deposited to the ProteomeXchange Consortium via the PRIDE partner repository with the dataset identifier PXD008005. This research was supported by NIH funding for the HIV Accessory and Regulatory Complexes (HARC) Center and UCSF-Gladstone Institute CFAR (P50GM082250, N.J.K., A.M., R.M.S. and J.D.G.; P30-AI027763, R.H.). S.H.C. is recipient of a UCSF-Zaffaroni fellowship and Ministry of Education fellowship (Taiwan). R.H. received postdoctoral fellowships from the Swiss National Science Foundation (P2EZP3_148742; P300P3_151154), the European Molecular Biology Organization (ALTF 1123-2013), and the Human Frontiers in Science Program (LT000089/2014-L). N.J.K. is supported by NIH funding (R01 AI120694). A.M. holds a Career Award for Medical Scientists from the Burroughs Wellcome Fund and is a Chan Zuckerberg Biohub Investigator. JH was supported by UCSF MSTP (T32GM007618).

Author contributions

S-HC and NJK conceived of the project. S-HC designed and performed experiments, and NJK supervised the research. S-HC and GMJ performed comparative proteomics on CRL4^{AMBRA1} with scoring assistance from RH. JRJ, BWN, and TLJ prepared MS samples, performed machine runs, and conducted database searching. JY generated and characterized ATG-knockout lines. KMR generated and characterized CUL4A-knockout lines. S-HC generated stable cell lines, and performed tandem IPs, single IPs, cell-based ubiquitination assays, immunoblotting, and co-transfection experiments. S-HC conducted IL-6-stimulation experiments, generated AMBRA1-knockout lines, and performed genotyping with assistance from DD. DEG, JH, and JFH isolated human primary T cells and performed HIV-1 infection assays with support from AM. Y-LL purified AMBRA1-DDB1 recombinant proteins from insect cells under the supervision of RMS. LAB purified proteins and performed in vitro ubiquitination assays with the guidance of JDG. S-HC wrote the manuscript with NJK with input from JD and JDG. S-HC, GMJ, DD, and RH edited the manuscript for publication.

Conflict of interest

A.M. serves as an advisor to Juno Therapeutics and PACT Therapeutics and is a founder of Spotlight Therapeutics, and the Marson laboratory has received sponsored research support from Juno Therapeutics and Epinomics. A patent has been filed on the use of Cas9 RNPs to edit the genome of human primary T cells (A.M.).

References

- Abbas T, Mueller AC, Shibata E, Keaton M, Rossi M, Dutta A (2013) CRL1-FBXO11 promotes Cdt2 ubiquitylation and degradation and regulates Pr-Set7/Set8-mediated cellular migration. *Mol Cell* 49: 1147–1158
- Angers S, Li T, Yi X, MacCoss MJ, Moon RT, Zheng N (2006) Molecular architecture and assembly of the DDB1–CUL4A ubiquitin ligase machinery. *Nature* 443: 590–593
- Antonoli M, Albiero F, Nazio F, Vescovo T, Perdomo AB, Corazzari M, Marsella C, Piselli P, Gretzmeier C, Dengjel J, Cecconi F, Piacentini M, Fimia GM (2014) AMBRA1 interplay with cullin E3 ubiquitin ligases regulates autophagy dynamics. *Dev Cell* 31: 734–746
- Babon JJ, Sabo JK, Zhang J-G, Nicola NA, Norton RS (2009) The SOCS box encodes a hierarchy of affinities for cullin 5: implications for ubiquitin ligase formation and cytokine signalling suppression. *J Mol Biol* 387: 162–174
- Bennett EJ, Rush J, Gygi SP, Harper JW (2010) Dynamics of cullin-RING ubiquitin ligase network revealed by systematic quantitative proteomics. *Cell* 143: 951–965
- de Bie P, Ciechanover A (2011) Ubiquitination of E3 ligases: self-regulation of the ubiquitin system via proteolytic and non-proteolytic mechanisms. *Cell Death Differ* 18: 1393–1402
- Boyle K, Egan P, Rakar S, Willson TA, Wicks IP, Metcalf D, Hilton DJ, Nicola NA, Alexander WS, Roberts AW, Robb L (2007) The SOCS box of suppressor of cytokine signaling-3 contributes to the control of G-CSF responsiveness *in vivo*. *Blood* 110: 1466–1474
- Brinkman EK, Chen T, Amendola M, van Steensel B (2014) Easy quantitative assessment of genome editing by sequence trace decomposition. *Nucleic Acids Res* 42: e168
- Choi M, Chang C-Y, Clough T, Broudy D, Killeen T, MacLean B, Vitek O (2014) MSstats: an R package for statistical analysis of quantitative mass spectrometry-based proteomic experiments. *Bioinformatics* 30: 2524–2526
- Cong L, Ran FA, Cox D, Lin S, Barretto R, Habib N, Hsu PD, Wu X, Jiang W, Marraffini LA, Zhang F (2013) Multiplex genome engineering using CRISPR/Cas systems. *Science* 339: 819–823
- Cox J, Mann M (2008) MaxQuant enables high peptide identification rates, individualized p.p.b.-range mass accuracies and proteome-wide protein quantification. *Nat Biotechnol* 26: 1367–1372
- Croker BA, Krebs DL, Zhang J-G, Wormald S, Willson TA, Stanley EG, Robb L, Greenhalgh CJ, Förster I, Clausen BE, Nicola NA, Metcalf D, Hilton DJ, Roberts AW, Alexander WS (2003) SOCS3 negatively regulates IL-6 signaling *in vivo*. *Nat Immunol* 4: 540–545
- Decorsière A, Mueller H, van Breugel PC, Abdul F, Gerossier L, Beran RK, Livingston CM, Niu C, Fletcher SP, Hantz O, Strubin M (2016) Hepatitis B virus X protein identifies the Smc5/6 complex as a host restriction factor. *Nature* 531: 386–389
- Du D, Katsuno Y, Meyer D, Budi EH, Chen SH, Koeppen H, Wang H, Akhurst RJ, Derynck R (2017) Smad3-mediated recruitment of the methyltransferase SETDB1/ESET controls Snail1 expression and epithelial-mesenchymal transition. *EMBO Rep* 19: 135–155
- Duda DM, Olszewski JL, Tron AE, Hammel M, Lambert LJ, Waddell MB, Mittag T, DeCaprio JA, Schulman BA (2012) Structure of a glomulin-RBX1-CUL1 complex: inhibition of a RING E3 ligase through masking of its E2-binding surface. *Mol Cell* 47: 371–382
- Duda DM, Borg LA, Scott DC, Hunt HW, Hammel M, Schulman BA (2008) Structural insights into NEDD8 activation of cullin-RING ligases: conformational control of conjugation. *Cell* 134: 995–1006
- Enchev RI, Scott DC, da Fonseca Paula CA, Schreiber A, Monda JK, Schulman BA, Peter M, Morris EP (2012) Structural basis for a reciprocal regulation between SCF and CSN. *Cell Rep* 2: 616–627
- Fischer ES, Scrima A, Böhm K, Matsumoto S, Lingaraju GM, Faty M, Yasuda T, Cavadini S, Wakasugi M, Hanaoka F, Iwai S, Gut H, Sugawara K, Thomä NH (2011) The molecular basis of CRL4DDB2/CSA ubiquitin ligase architecture, targeting, and activation. *Cell* 147: 1024–1039
- Fischer ES, Böhm K, Lydeard JR, Yang H, Stadler MB, Cavadini S, Nagel J, Serluca F, Acker V, Lingaraju GM, Tichkule RB, Schebesta M, Forrester WC,

- Schirle M, Hassiepen U, Ottl J, Hild M, Beckwith RE, Harper JW, Jenkins JL et al (2014) Structure of the DDB1-CRBN E3 ubiquitin ligase in complex with thalidomide. *Nature* 512: 49–53
- Foe IT, Foster SA, Cheung SK, DeLuca SZ, Morgan DO, Toczyski DP (2011) Ubiquitination of Cdc20 by the APC occurs through an intramolecular mechanism. *Curr Biol* 21: 1870–1877
- Frescas D, Pagano M (2008) Deregulated proteolysis by the F-box proteins SKP2 and β -TrCP: tipping the scales of cancer. *Nat Rev Cancer* 8: 438–449
- Galan J-M, Peter M (1999) Ubiquitin-dependent degradation of multiple F-box proteins by an autocatalytic mechanism. *Proc Natl Acad Sci USA* 96: 9124–9129
- Geng J, Klionsky DJ (2008) The Atg8 and Atg12 ubiquitin-like conjugation systems in macroautophagy. 'Protein modifications: beyond the usual suspects' review series. *EMBO Rep* 9: 859–864
- Geyer R, Wee S, Anderson S, Yates J, Wolf DA (2003) BTB/POZ domain proteins are putative substrate adaptors for cullin 3 ubiquitin ligases. *Mol Cell* 12: 783–790
- Guo Y, Dong L, Qiu X, Wang Y, Zhang B, Liu H, Yu Y, Zang Y, Yang M, Huang Z (2014) Structural basis for hijacking CBF- β and CUL5 E3 ligase complex by HIV-1 Vif. *Nature* 505: 229–233
- He YJ, McCall CM, Hu J, Zeng Y, Xiong Y (2006) DDB1 functions as a linker to recruit receptor WD40 proteins to CUL4-ROC1 ubiquitin ligases. *Genes Dev* 20: 2949–2954
- Hicke L, Dunn R (2003) Regulation of membrane protein transport by ubiquitin and ubiquitin-binding proteins. *Annu Rev Cell Dev Biol* 19: 141–172
- Hultquist JF, Schumann K, Woo JM, Manganaro L, McGregor MJ, Doudna J, Simon V, Krogan NJ, Marson A (2016) A Cas9 ribonucleoprotein platform for functional genetic studies of HIV-host interactions in primary human T cells. *Cell Rep* 17: 1438–1452
- Jäger S, Cimermancic P, Gulbahce N, Johnson JR, McGovern KE, Clarke SC, Shales M, Mercenne G, Pache L, Li K, Hernandez H, Jang GM, Roth SL, Akiva E, Marlett J, Stephens M, D'Orso I, Fernandes J, Fahey M, Mahon C et al (2011a) Global landscape of HIV-human protein complexes. *Nature* 481: 365–370
- Jäger S, Gulbahce N, Cimermancic P, Kane J, He N, Chou S, D'Orso I, Fernandes J, Jang G, Frankel AD, Alber T, Zhou Q, Krogan NJ (2011b) Purification and characterization of HIV-human protein complexes. *Methods* 53: 13–19
- Jäger S, Kim DY, Hultquist JF, Shindo K, LaRue RS, Kwon E, Li M, Anderson BD, Yen L, Stanley D, Mahon C, Kane J, Franks-Skiba K, Cimermancic P, Burlingame A, Sali A, Craik CS, Harris RS, Gross JD, Krogan NJ (2011c) Vif hijacks CBF- β to degrade APOBEC3G and promote HIV-1 infection. *Nature* 481: 371–375
- Jin J, Arias EE, Chen J, Harper JW, Walter JC (2006) A family of diverse Cul4-Ddb1-interacting proteins includes Cdt2, which is required for S phase destruction of the replication factor Cdt1. *Mol Cell* 23: 709–721
- Kane JR, Stanley DJ, Hultquist JF, Johnson JR, Mietrach N, Binning JM, Jonsson SR, Barelier S, Newton BW, Johnson TL, Franks-Skiba KE, Li M, Brown WL, Gunnarsson HI, Adalbjornsdottir A, Fraser JS, Harris RS, Andresdottir V, Gross JD, Krogan NJ (2015) Lineage-specific viral hijacking of Non-canonical E3 ubiquitin ligase cofactors in the evolution of Vif anti-APOBEC3 activity. *Cell Rep* 11: 1236–1250
- Kershaw NJ, Laktyushin A, Nicola NA, Babon JJ (2014) Reconstruction of an active SOCS3-based E3 ubiquitin ligase complex *in vitro*: identification of the active components and JAK2 and gp130 as substrates. *Growth Factors* 32: 1–10
- Kim W, Bennett EJ, Huttlin EL, Guo A, Li J, Possemato A, Sowa ME, Rad R, Rush J, Comb MJ, Harper JW, Gygi SP (2011) Systematic and quantitative assessment of the ubiquitin-modified proteome. *Mol Cell* 44: 325–340
- Klionsky DJ, Abdelmohsen K, Abe A, Abedin MJ, Abeliovich H, Arozena AA, Adachi H, Adams CM, Adams PD, Adeli K, Adhietty PJ, Adler SG, Agam G, Agarwal R, Aghi MK, Agnello M, Agostinis P, Aguilar PV, Aguirre-Ghiso J, Airolidi EM et al (2016) Guidelines for the use and interpretation of assays for monitoring autophagy (3rd edition). *Autophagy* 12: 1–222
- Koepp DM, Schaefer LK, Ye X, Keyomarsi K, Chu C, Harper JW, Elledge SJ (2001) Phosphorylation-dependent ubiquitination of cyclin E by the SCFFbw7 ubiquitin ligase. *Science* 294: 173–177
- Lang R, Pauleau A-L, Parganas E, Takahashi Y, Mages J, Ihle JN, Rutschman R, Murray PJ (2003) SOCS3 regulates the plasticity of gp130 signaling. *Nat Immunol* 4: 546–550
- Lecossier D, Bouchonnet F, Clavel F, Hance AJ (2003) Hypermutation of HIV-1 DNA in the absence of the Vif protein. *Science* 300: 1112
- Lingaraju GM, Bunker RD, Cavadini S, Hess D, Hassiepen U, Renatus M, Fischer ES, Thomä NH (2014) Crystal structure of the human COP9 signalosome. *Nature* 512: 161–165
- Lisztwan J, Imbert G, Wirbelauer C, Gstaiger M, Krek W (1999) The von Hippel-Lindau tumor suppressor protein is a component of an E3 ubiquitin-protein ligase activity. *Genes Dev* 13: 1822–1833
- Luo Y, Jacobs EY, Greco TM, Mohammed KD, Tong T, Keegan S, Binley JM, Cristea IM, Fenyö D, Rout MP, Chait BT, Muesing MA (2016) HIV-host interactome revealed directly from infected cells. *Nat Microbiol* 1: 16068
- Mahon C, Krogan NJ, Craik CS, Pick E (2014) Cullin E3 ligases and their rewiring by viral factors. *Biomolecules* 4: 897–930
- Maria Fimia G, Stoykova A, Romagnoli A, Giunta L, Di Bartolomeo S, Nardacci R, Corazzari M, Fuoco C, Ucar A, Schwartz P, Gruss P, Piacentini M, Chowdhury K, Cecconi F (2007) Ambra1 regulates autophagy and development of the nervous system. *Nature* 447: 1121–1125
- Mehle A, Goncalves J, Santa-Marta M, McPike M, Gabuzda D (2004) Phosphorylation of a novel SOCS-box regulates assembly of the HIV-1 Vif-Cul5 complex that promotes APOBEC3G degradation. *Genes Dev* 18: 2861–2866
- Muller B, Daecke J, Fackler OT, Dittmar MT, Zentgraf H, Krausslich HG (2004) Construction and characterization of a fluorescently labeled infectious human immunodeficiency virus type 1 derivative. *J Virol* 78: 10803–10813
- Nathans R, Cao H, Sharova N, Ali A, Sharkey M, Stranska R, Stevenson M, Rana TM (2008) Small-molecule inhibition of HIV-1 Vif. *Nat Biotechnol* 26: 1187–1192
- Olma MH, Roy M, Le Bihan T, Sumara I, Maerki S, Larsen B, Quadroni M, Peter M, Tyers M, Pintard L (2009) An interaction network of the mammalian COP9 signalosome identifies Dda1 as a core subunit of multiple Cul4-based E3 ligases. *J Cell Sci* 122: 1035–1044
- Petroski MD, Deshaies RJ (2005) Function and regulation of cullin-RING ubiquitin ligases. *Nat Rev Mol Cell Biol* 6: 9–20
- Petzold G, Fischer ES, Thoma NH (2016) Structural basis of lenalidomide-induced CK1 α degradation by the CRL4(CRBN) ubiquitin ligase. *Nature* 532: 127–130
- Pierce NW, Lee JE, Liu X, Sweredoski MJ, Graham RL, Larimore EA, Rome M, Zheng N, Clurman BE, Hess S, Shan SO, Deshaies RJ (2013) Cand1 promotes assembly of new SCF complexes through dynamic exchange of F box proteins. *Cell* 153: 206–215
- Pozzebon ME, Varadaraj A, Mattosio D, Jaffray EG, Miccolo C, Galimberti V, Tommasino M, Hay RT, Chiocca S (2013) BC-box protein domain-related mechanism for VHL protein degradation. *Proc Natl Acad Sci USA* 110: 18168–18173

- Richards C, Albin JS, Demir Ö, Shaban NM, Luengas EM, Land AM, Anderson BD, Holten JR, Anderson JS, Harki DA, Amaro RE, Harris RS (2015) The binding interface between human APOBEC3F and HIV-1 Vif elucidated by genetic and computational approaches. *Cell Rep* 13: 1781–1788
- Rossi M, Duan S, Jeong YT, Horn M, Saraf A, Florens L, Washburn MP, Antebi A, Pagano M (2013) Regulation of the CRL4(Cdt2) ubiquitin ligase and cell-cycle exit by the SCF(Fbxo11) ubiquitin ligase. *Mol Cell* 49: 1159–1166
- Schmidt MW, McQuary PR, Wee S, Hofmann K, Wolf DA (2009) F-Box-directed CRL complex assembly and regulation by the CSN and CAND1. *Mol Cell* 35: 586–597
- Shannon P, Markiel A, Ozier O, Baliga NS, Wang JT, Ramage D, Amin N, Schwikowski B, Ideker T (2003) Cytoscape: a software environment for integrated models of biomolecular interaction networks. *Genome Res* 13: 2498–2504
- Sowa ME, Bennett EJ, Gygi SP, Harper JW (2009) Defining the human deubiquitinating enzyme interaction landscape. *Cell* 138: 389–403
- Stebbins CE, Kaelin WG Jr, Pavletich NP (1999) Structure of the VHL-ElonginC-ElonginB complex: implications for VHL tumor suppressor function. *Science* 284: 455–461
- Team RC (2015) *R: a language and environment for statistical computing*. Vienna, Austria: R Foundation for Statistical Computing
- Teo G, Liu G, Zhang J, Nesvizhskii AI, Gingras AC, Choi H (2014) SAINTExpress: improvements and additional features in significance analysis of INTeractome software. *J Proteomics* 100: 37–43
- Tron AE, Arai T, Duda DM, Kuwabara H, Olszewski JL, Fujiwara Y, Bahamon BN, Signoretti S, Schulman BA, DeCaprio JA (2012) The glomulin malformation protein Glomulin binds Rbx1 and regulates cullin RING ligase-mediated turnover of Fbw7. *Mol Cell* 46: 67–78
- Wee S, Geyer RK, Toda T, Wolf DA (2005) CSN facilitates Cullin–RING ubiquitin ligase function by counteracting autocatalytic adapter instability. *Nat Cell Biol* 7: 387–391
- Weissman AM, Shabek N, Ciechanover A (2011) The predator becomes the prey: regulating the ubiquitin system by ubiquitylation and degradation. *Nat Rev Mol Cell Biol* 12: 605–620
- Welcker M, Larimore EA, Swanger J, Bengoechea-Alonso MT, Grim JE, Ericsson J, Zheng N, Clurman BE (2013) Fbw7 dimerization determines the specificity and robustness of substrate degradation. *Genes Dev* 27: 2531–2536
- Xia P, Wang S, Du Y, Zhao Z, Shi L, Sun L, Huang G, Ye B, Li C, Dai Z, Hou N, Cheng X, Sun Q, Li L, Yang X, Fan Z (2013) WASH inhibits autophagy through suppression of Beclin 1 ubiquitination. *EMBO J* 32: 2685–2696
- Xia P, Wang S, Huang G, Du Y, Zhu P, Li M, Fan Z (2014) RNF2 is recruited by WASH to ubiquitinate AMBRA1 leading to downregulation of autophagy. *Cell Res* 24: 943–958
- Yoshimura A, Naka T, Kubo M (2007) SOCS proteins, cytokine signalling and immune regulation. *Nat Rev Immunol* 7: 454–465
- Yu X, Yu Y, Liu B, Luo K, Kong W, Mao P, Yu X-F (2003) Induction of APOBEC3G ubiquitination and degradation by an HIV-1 Vif-Cul5-SCF complex. *Science* 302: 1056–1060
- Yu H, Pardoll D, Jove R (2009) STATs in cancer inflammation and immunity: a leading role for STAT3. *Nat Rev Cancer* 9: 798–809
- Zhang J-G, Metcalf D, Rakar S, Asimakis M, Greenhalgh CJ, Willson TA, Starr R, Nicholson SE, Carter W, Alexander WS, Hilton DJ, Nicola NA (2001) The SOCS box of suppressor of cytokine signaling-1 is important for inhibition of cytokine action *in vivo*. *Proc Natl Acad Sci USA* 98: 13261–13265
- Zhou P, Howley PM (1998) Ubiquitination and degradation of the substrate recognition subunits of SCF ubiquitin–protein ligases. *Mol Cell* 2: 571–580